



# Development and evaluation of an advanced National Air Quality Forecasting Capability using the NOAA Global Forecast System version 16

Patrick C. Campbell<sup>1,2</sup>, Youhua Tang<sup>1,2</sup>, Pius Lee<sup>1,☆</sup>, Barry Baker<sup>1</sup>, Daniel Tong<sup>1,2</sup>, Rick Saylor<sup>1</sup>, Ariel Stein<sup>1</sup>, Jianping Huang<sup>3,4</sup>, Ho-Chun Huang<sup>3,4</sup>, Edward Strobach<sup>3,4</sup>, Jeff McQueen<sup>3</sup>, Li Pan<sup>3,4</sup>, Ivanka Stajner<sup>3</sup>, James Sims<sup>5</sup>, Jose Tirado-Delgado<sup>5,6</sup>, Youngsun Jung<sup>5</sup>, Fanglin Yang<sup>3</sup>, Tanya L. Spero<sup>7</sup>, and Robert C. Gilliam<sup>7</sup>

<sup>1</sup>NOAA Air Resources Laboratory (ARL), College Park, MD, USA

<sup>2</sup>Center for Spatial Information Science and Systems, George Mason University, Fairfax, VA, USA

<sup>3</sup>NOAA National Centers for Environmental Prediction (NCEP), College Park, MD, USA

<sup>4</sup>I.M. Systems Group Inc., Rockville, MD, USA

<sup>5</sup>NOAA NWS/STI, College Park, MD, USA

<sup>6</sup>Eastern Research Group, Inc. (ERG), College Park, MD, USA

<sup>7</sup>US Environmental Protection Agency, Research Triangle Park, NC, USA

☆retired

**Correspondence:** Patrick C. Campbell (patrick.c.campbell@noaa.gov)

Received: 14 September 2021 – Discussion started: 26 October 2021

Revised: 7 March 2022 – Accepted: 8 March 2022 – Published: 21 April 2022

**Abstract.** A new dynamical core, known as the Finite-Volume Cubed-Sphere (FV3) and developed at both NASA and NOAA, is used in NOAA's Global Forecast System (GFS) and in limited-area models for regional weather and air quality applications. NOAA has also upgraded the operational FV3GFS to version 16 (GFSv16), which includes a number of significant developmental advances to the model configuration, data assimilation, and underlying model physics, particularly for atmospheric composition to weather feedback. Concurrent with the GFSv16 upgrade, we couple the GFSv16 with the Community Multiscale Air Quality (CMAQ) model to form an advanced version of the National Air Quality Forecasting Capability (NAQFC) that will continue to protect human and ecosystem health in the US. Here we describe the development of the FV3GFSv16 coupling with a “state-of-the-science” CMAQ model version 5.3.1. The GFS–CMAQ coupling is made possible by the seminal version of the NOAA-EPA Atmosphere–Chemistry Coupler (NACC), which became a major piece of the next operational NAQFC system (i.e., NACC-CMAQ) on 20 July 2021. NACC-CMAQ has a number of scientific advancements that include satellite-based data acquisition tech-

nology to improve land cover and soil characteristics and inline wildfire smoke and dust predictions that are vital to predictions of fine particulate matter (PM<sub>2.5</sub>) concentrations during hazardous events affecting society, ecosystems, and human health. The GFS-driven NACC-CMAQ model has significantly different meteorological and chemical predictions compared to the previous operational NAQFC, where evaluation of NACC-CMAQ shows generally improved near-surface ozone and PM<sub>2.5</sub> predictions and diurnal patterns, both of which are extended to a 72 h (3 d) forecast with this system.

## 1 Introduction

Air quality is defined as the degree to which the ambient air is free of pollutants – which are either directly emitted into the atmosphere (primary air pollutants) or formed within the atmosphere itself (secondary air pollutants) – that cause degradation to human health, visibility, and/or ecological systems (WHO, 2006). Air quality is as ubiquitous and important as weather impacts, where outdoor air pollution is globally re-

sponsible for  $\sim 4.2$  million early deaths each year ([https://www.who.int/health-topics/air-pollution#tab=tab\\_1](https://www.who.int/health-topics/air-pollution#tab=tab_1), last access: 5 April 2022). To put this into perspective, this is over 3 times the number of people who die from HIV/AIDS and over 8 times the number of homicides each year (2017 Global Burden of Disease Study: <https://www.thelancet.com/gbd>, last access: 5 April 2022). Air pollution is costly and leads to huge economic damage (Landrigan et al., 2018). There are also disproportionate impacts of air pollution across poorer people and some racial and ethnic groups, who are among those who often face higher exposure and potential responses to pollutants (Institute of Medicine, 1999; American Lung Association, 2001; O’Neil et al., 2003; Finkelstein et al., 2003; Zeka et al., 2006).

Air pollutants are composed of both gaseous and particulate species, which under prolonged exposure can cause non-carcinogenic (Lee et al., 2014) and/or carcinogenic adverse health effects (Demetirou and Vineis, 2015). High ground-level ozone ( $O_3$ ) concentrations (i.e., smog), for example, can lead to decreased lung function and cause respiratory symptoms. These symptoms are particularly dangerous for sensitive groups such as young children, the elderly, and those with preexisting conditions that include asthma, chronic obstructive pulmonary disease (COPD), lung cancer, and respiratory infection (Kar Kurt et al., 2016).

To protect against the health and environmental impacts of air pollution, world agencies have developed regulations and standards on the allowable amount of primary and secondary air pollution measured at different spatiotemporal scales (e.g., seconds to months and local to global scales), which largely depend on the atmospheric lifetime of specific air components (WHO, 2005, 2010). Typically, the world’s most extreme air pollution occurs near global megacities where population density is highest (Marlier et al., 2016). Rapid economic growth in China, for example, has led to extremely high air pollution levels over the past decade (Zhou et al., 2017; Liu and Wang, 2020), necessitating significant efforts to implement air pollution prevention and control plans (Chinese State Council, 2013; Zhao et al., 2017). The US Environmental Protection Agency (EPA) defines ambient concentration limits for primary pollutants such as sulfur dioxide ( $SO_2$ ), oxides of nitrogen ( $NO_x=NO+NO_2$ ), carbon monoxide (CO), lead (Pb), and total (carbonaceous and non-carbonaceous) particulate matter (PM). Other important primary pollutants include total volatile organic compounds (VOCs), which have many sources (both natural and anthropogenic) and serve as vital precursor gases to secondary pollutants such as ground-level  $O_3$  and the formation of fine particulate matter with an aerodynamic diameter of less than  $2.5\ \mu m$  ( $PM_{2.5}$ ). Ground-level  $O_3$  and  $PM_{2.5}$  are two of the six US EPA “criteria pollutants” that are regulated for their concentrations, exposure level, and health impacts. This is largely because there is a relatively mature understanding of their sources, formation, and characteristics (e.g., Sillman et al., 1990; Sillman, 1995, 1999; Pinder et al., 2008; Kim et

al., 2011a, b; Zhang et al., 2009a, b; Campbell et al., 2015; Karamchandani et al., 2017). There is also a widespread ability to compare observed and simulated ambient ozone concentrations over both short-term (McKeen et al., 2005, 2007, 2009) and dynamic long-term periods (e.g., Astitha et al., 2017), which has helped lead to an understanding of their well-attributable health impacts (e.g., WHO, 2006; Sun et al., 2015; Zhang et al., 2018).

To address prolific air pollution concerns in the US during the 1950s–1960s, the first development and application of real-time air quality forecast (RT-AQF) models began in the 1970s–1980s (i.e., the first- and second-generation air quality models) coincident with the establishment of the US EPA by President Nixon. Initially the models were based on empirical approaches and statistical models (Zhang et al., 2012a); however, by the 1990s and early 2000s, RT-AQF models underwent a significant evolution and evolved to more complex 3-D numerical air quality models (third- and fourth-generation air quality models). These RT-AQF models involved more sophisticated techniques, including increasingly complex parameterizations and chemistry, bias-correction methods and data fusion, chemical data assimilation, and hybrid statistical or numerical methods with artificial intelligence and machine learning algorithms to improve RT-AQF model efficiency and predictions (Zhang et al., 2012b; Bai et al., 2018). RT-AQF models have become vital tools to improve our understanding and prediction of how air pollutants form, disperse, and deposit to the surface and are used by local health and air managers to assess the air quality conditions to make informed decisions on mitigation measures to reduce public exposure.

To address the nation’s need for reducing the adverse health effects of air pollution and associated costly medical expenses, in 2002 Congress addressed the National Oceanic and Atmospheric Administration (NOAA) to provide National AQF guidance (H.R. Energy Policy Act of 2002 – Senate Amendment S. 517, SA1383, Forecasts and Warnings). A joint project emerged from this amendment between NOAA and the EPA to develop and establish the initial phase of a RT-AQF system, which consisted of the coupled NOAA’s ETA meteorological model (Black, 1994; Rogers et al., 1996) with EPA’s Models-3 Community Multiscale Air Quality (CMAQ) model (Byun and Ching, 1999; Byun and Schere, 2006). This “offline-coupled” model provided  $O_3$  forecast guidance for the northeastern US states (Kang et al., 2005; Otte et al., 2005; Eder et al., 2006) and formed the early version of the National Air Quality Forecasting Capability (NAQFC) that was first implemented for operations in September 2004 ([https://www.weather.gov/sti/stimodeling\\_airquality\\_predictions](https://www.weather.gov/sti/stimodeling_airquality_predictions), last access: 5 April 2022). The NAQFC was further developed at NOAA and collaborating laboratories (Mathur et al., 2008; McKeen et al., 2005, 2007, 2009) and was comprehensively evaluated in Eder et al. (2009). The NAQFC has been continuously advanced to provide both  $O_3$  and  $PM_{2.5}$  forecast

guidance for the entire conterminous US (CONUS), has expanded its predictions to both Alaska and Hawaii, and has provided pivotal air quality forecast guidance to a multitude of stakeholders to help protect human health and the environment (Stajner et al., 2011; Lee et al., 2017; Huang et al., 2017). Prior to the advanced version described in this paper, the NAQFC used the offline-coupled North American Mesoscale Model Forecast System on the B-Grid (NMMB) (Black, 1994; Janjic and Gall, 2012) and CMAQv5.0.2 (US EPA, 2014). The NAQFC provides forecast guidance for O<sub>3</sub>, PM<sub>2.5</sub>, wildfire smoke, and dust at a horizontal grid spacing of 12 km over a domain centered on the CONUS, Alaska, and Hawaii domains.

NOAA's National Weather Service (NWS) transitioned operationally in June 2019 to use a new dynamical core known as the Finite-Volume Cubed-Sphere (FV3) in the Global Forecast System (GFS) model. Both the National Aeronautics and Space Administration (NASA) and NOAA's Geophysical Fluid Dynamics Laboratory (GFDL; <https://www.gfdl.noaa.gov/>, last access: 5 April 2022) have developed and advanced FV3 over the past few decades (Lin et al., 1994; Lin and Rood, 1996; Lin, 2004; Putman and Lin, 2007; Chen et al., 2013; Harris and Lin, 2013; Harris et al., 2016; Zhou et al., 2019). Overall, the switch to a FV3-based dynamical core with advancements to GFS's observation quality control, data assimilation, and model physical parameterizations (from the National Center for Environmental Prediction) significantly increases the accuracy of 1–2 d and longer (e.g., 3–7 d) weather forecasts (Chen et al., 2019). Other advantages of FV3GFS are improved computational efficiency and adaptable scaling, enhanced and flexible vertical resolution, and improved representation of atmospheric circulation and weather patterns across different horizontal scales (Yang et al., 2020; [https://www.weather.gov/media/notification/pns20-44gfs\\_v16.pdf](https://www.weather.gov/media/notification/pns20-44gfs_v16.pdf), last access: 5 April 2022; [https://www.emc.ncep.noaa.gov/emc/pages/numerical\\_forecast\\_systems/gfs.php](https://www.emc.ncep.noaa.gov/emc/pages/numerical_forecast_systems/gfs.php), last access: 5 April 2022; [https://ufsccommunity.org/wp-content/uploads/2020/10/UFS\\_Webnair\\_GFSv16\\_20201022\\_FanglinYang.pdf](https://ufsccommunity.org/wp-content/uploads/2020/10/UFS_Webnair_GFSv16_20201022_FanglinYang.pdf), last access: 5 April 2022).

The improved representation of atmospheric conditions, circulation, transport, and precipitation in GFS are pivotal to the accuracy of chemical predictions when coupled to RT-AQF models. Since 2017, there has also been significant efforts at NOAA to use version 15 of FV3GFS (hereafter, GFSv15) rather than NMMB as the meteorological driver for CMAQ in the NAQFC (Huang et al., 2017, 2018, 2019). Huang et al. (2020) and Chen et al. (2021) demonstrated that a version of the GFS-driven CMAQv5.0.2 (GFSv15-CMAQ) forecasting system had partly improved O<sub>3</sub> predictions compared to the NMMB-driven CMAQ (NMMB-CMAQ) system but that the GFSv15-CMAQ had large biases for PM<sub>2.5</sub> that still need improvement.

Concurrently, at NOAA there has been a major upgrade of GFS from version 15 to 16 (GFSv16), which includes

a number of major developmental advances to the system (see Sect. 2 of this paper). Thus, there was an opportunity to simultaneously upgrade and streamline the meteorological coupling between the GFSv16 and a more updated, “state-of-the-science” version of CMAQ at the US EPA (US EPA, 2019; Appel et al., 2021). The current CMAQv5.0.2 used in the NMMB-CMAQ and experimental GFSv15-CMAQ is outdated scientifically with numerous deficiencies, many of which led to the elevated biases and error as described in Huang et al. (2017, 2020) and Chen et al. (2021). Hence, there is a need to update the NAQFC to actively developing versions of both FV3GFS and CMAQ.

The main objectives of this paper are to describe the development of the GFSv16 coupling with a state-of-the-science CMAQ model for the advanced updates to NAQFC that includes numerous other RT-AQF science advances (Sect. 2). We also describe the new simulation design and input observations, and evaluate the meteorological and air quality predictions across the US compared to the now discontinued NMMB-CMAQ system for NAQFC (Sects. 3 and 4). We conclude with a summary of NOAA-EPA Atmosphere Chemistry Coupler (NACC)-CMAQ serving as the current (since 20 July 2021) operational NAQFC, as well as longer-term goals (Sect. 5). We hypothesize that advancing to closer state-of-the-science meteorological and chemical transport models will improve atmospheric chemical composition predictions, and the resulting air quality forecasts will better protect human health across the US.

## 2 Methods

### 2.1 Updated meteorological and surface drivers

#### 2.1.1 The Global Forecast System version 16

The Environmental Modeling Center (EMC) at NOAA continuously develops and improves the GFS model, which has been in operation at the National Weather Service since 1980. EMC has recently upgraded the GFS model from v15.3 to v16 in February 2021, and the major upgrade improves the model forecast performance while also providing enhanced forecast products. Some of the major structural changes to GFSv16 (compared to previous GFS versions) include increased vertical layers (resolution) from 64 to 127 (Fig. 1) and an extended model top from 54 (upper stratosphere) to 80 km (mesopause). GFSv16 also has a thinner first model layer thickness (20 m) and higher-resolution global horizontal grids of ~25 and 13 km (Yang et al., 2020; [https://www.weather.gov/media/notification/pns20-44gfs\\_v16.pdf](https://www.weather.gov/media/notification/pns20-44gfs_v16.pdf), last access: 5 April 2022; [https://www.emc.ncep.noaa.gov/emc/pages/numerical\\_forecast\\_systems/gfs.php](https://www.emc.ncep.noaa.gov/emc/pages/numerical_forecast_systems/gfs.php), last access: 5 April 2022; <https://ufsccommunity.org/wp-content/uploads/2020/10/>

UFS\_Webnair\_GFSv16\_20201022\_FanglinYang.pdf, last access: 5 April 2022).

The GFSv16 has significantly improved its physical parameterizations (e.g., planetary boundary layer (PBL), gravity wave, radiation, clouds and precipitation, land surface, and surface layer schemes) and upgraded to the Global Data Assimilation System (GDAS) version 16 (Yang et al., 2020; [https://www.weather.gov/media/notification/pns20-44gfs\\_v16.pdf](https://www.weather.gov/media/notification/pns20-44gfs_v16.pdf), last access: 5 April 2022; [https://www.emc.ncep.noaa.gov/emc/pages/numerical\\_forecast\\_systems/gfs.php](https://www.emc.ncep.noaa.gov/emc/pages/numerical_forecast_systems/gfs.php), last access: 5 April 2022; [https://ufsccommunity.org/wp-content/uploads/2020/10/UFS\\_Webnair\\_GFSv16\\_20201022\\_FanglinYang.pdf](https://ufsccommunity.org/wp-content/uploads/2020/10/UFS_Webnair_GFSv16_20201022_FanglinYang.pdf), last access: 5 April 2022).

The global GFSv16 has changed the format of forecast output history files from binary (nemsio) to netCDF with zlib compression (data volume reduced by about 60 %), and provides the hourly (important for CMAQ predictions) output for a 72 h (3 d) forecast each day. The prior operational NAQFC (NMMB-CMAQ) forecast is only out to 48 h (2 d). The netCDF output is available (via live disk and archives) to all of NOAA's downstream model applications and is in the form of a rectangular Gaussian grid with a globally uniform grid resolution of  $\sim 13$  km (referred to as "C768") and a set number of latitude and longitude coordinates. The NOAA GFDL website provides more information about FV3 and its grids (<https://www.gfdl.noaa.gov/fv3/>, last access: 5 April 2022). There are additional new surface fields in the GFSv16 output, which include plant canopy surface water, surface temperature and moisture at four below-ground levels (0–0.1, 0.1–0.4, 0.4–1, 1–2 m), surface roughness, soil and vegetation type, and friction velocity.

### 2.1.2 The NOAA-EPA Atmosphere Chemistry Coupler (NACC)

The meteorological–chemical coupling of the GFSv16 to the regional, state-of-the-science CMAQ v5.3.1 model (US EPA, 2019; Appel et al., 2021) is achieved via the NOAA-EPA Atmosphere Chemistry Coupler (NACC) version 1 (NACC, i.e., "knack", meaning an acquired skill), which is adapted from the US EPA's Meteorology–Chemistry Interface Processor (MCIP) version 5 (Otte and Pleim, 2010; <https://github.com/USEPA/CMAQ>, last access: 5 April 2022). The NACC and CMAQ coupling (hereafter referred to as NACC-CMAQ) involves a number of structural and scientific advancements (Fig. 2, i.e., the advanced NAQFC) compared to the previous operational NMMB-CMAQ; hereafter referred to as "prior NAQFC".

The major structural changes to NACC-CMAQ include a variable-dependent bilinear or nearest-neighbor horizontal interpolation of the GFSv16 Gaussian gridded ( $\sim 13$  km) fields (e.g., 2 m temperature, 2 m specific humidity, 10 m wind speed and direction, and sea level pressure) to a Lambert conic conformal (LCC) projection at 12 km horizontal

grid spacing (same as the prior NAQFC) (Fig. 3a–b). NACC-CMAQ also includes a redefined vertical structure based on vertical interpolation (i.e., collapsing) to a 35-layer configuration (Fig. 3c) that is identical to the prior NAQFC.

Time-splitting techniques based on message passing interface (MPI) commands parallelize the GFSv16-to-NACC input and output (IO), which vastly improves the computational efficiency for the updated 72 h forecast period. The NACC-CMAQ coupling is more unified and streamlined compared to prior NAQFC (Stajner et al., 2011; Lee et al., 2017; Huang et al., 2017) and experimental GFSv15-CMAQ (Huang et al., 2018, 2019) applications, while eliminating multiple pre- and post-processing steps. The NACC-CMAQ processing steps are therefore subject to less uncertainty that comes with multiple grid interpolations and restructuring used previously and are more computationally efficient for the 72 h forecast window. Furthermore, the vertical interpolation from 127 to 35 layers results in an excellent agreement in the vertical structure of key atmospheric state variables (Fig. 3c). While this example is only for the central US, other model grid cell locations in the eastern and western US also demonstrate excellent agreement in the native and collapsed vertical structure in NACC (not shown). While NACC-CMAQ domains for Alaska and Hawaii are also available for NAQFC, this paper focuses only on the results inside the CONUS domain.

The left side of Fig. 2 shows that NACC-CMAQ incorporates high-resolution satellite data for a 2018–2020 climatological (12-month) averaged leaf area index (LAI), which is based on the Visible Infrared Imager Radiometer Suite (VIIRS) 8 d, level 4 global 500 m sinusoidal (SIN) grid, V001 product (Myneni and Knyazikhin, 2018; <https://lpdaac.usgs.gov/products/vnp15a2hv001/>, last access: 5 April 2022). This is a substantial update from the prior NAQFC, which assumed an unrealistic static LAI value of 4 across the entire domain. The NOAA product for near-real-time (NRT) greenness vegetation fraction (GVF) from VIIRS (Ding and Zhu, 2018; <https://www.ospo.noaa.gov/Products/land/gvf/>, last access: 5 April 2022) is used as a dynamic, direct input in NACC-CMAQ instead of using the GFSv16 vegetation fraction (VEG). Both VIIRS LAI and GVF are preprocessed, and NACC performs nearest-neighbor interpolation to the NAQFC grid.

More realistic land cover characteristics have shown to improve modeled meteorology, chemistry, and surface–atmosphere exchange processes in the coupled Weather Research and Forecasting (WRF; Powers et al., 2017; Skamarock and Klemp, 2008) and CMAQ model (e.g., Ran et al., 2016; Campbell et al., 2019). Test results here show that rapid-refresh of high-resolution VIIRS LAI and GVF in NACC have distinct differences compared to an older 2010 MODIS International Geosphere–Biosphere Programme (IGBP) LAI climatology and GFSv16-based VEG, respectively (Figs. S1–S2 in the Supplement). The updated dynamic LAI and GVF alter biogenic emissions, dry depo-



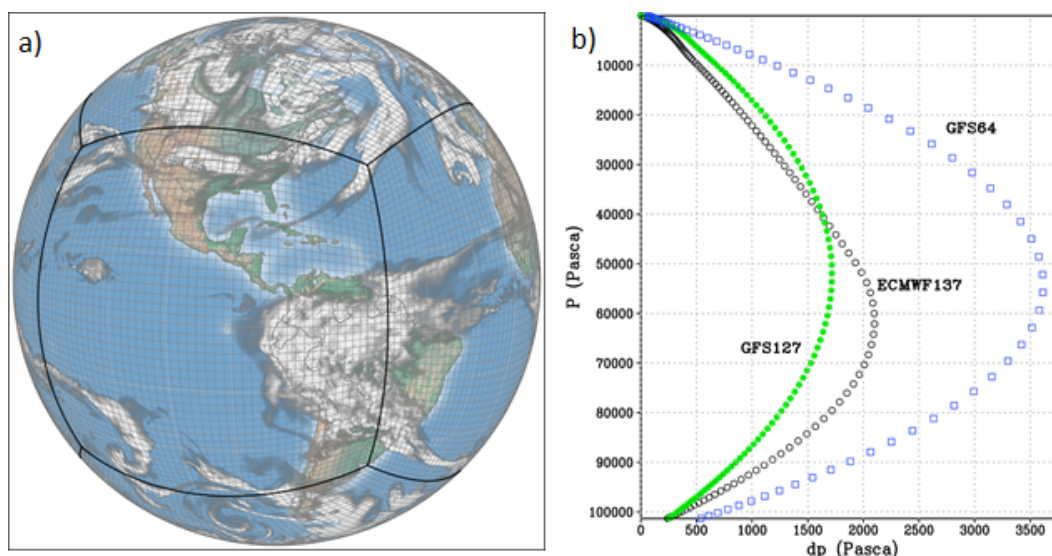


**Figure 1.** The (a) native FV3 gnomonic cubed-sphere grid at C48 ( $2^\circ$ ) resolution (image courtesy of Dusan Jovic, NOAA) and (b) vertical resolution ( $P$  vs.  $dp$ ) for the upgraded GFSv16 (green) compared to the previous GFSv15.3 (blue) and the European Centre for Medium-Range Weather Forecasts (ECMWF) model (black).

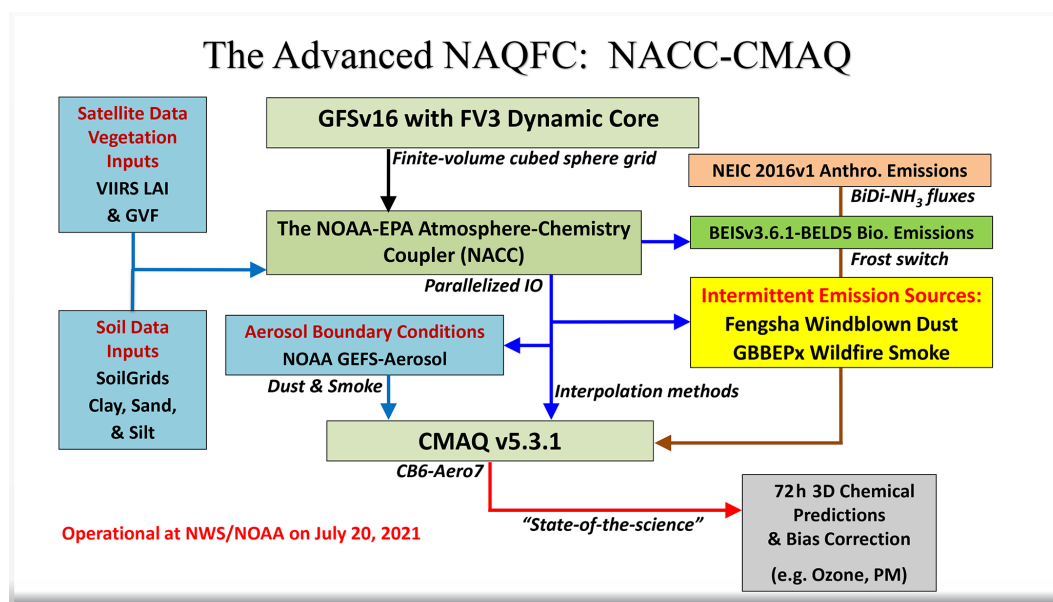


**Figure 2.** Schematic of the advanced NAQFC based on NACC-CMAQ.

sition, and resulting concentrations of gases and aerosols in NACC-CMAQ, particularly during the fall transition month of October 2020 (Fig. S3).

NACC-CMAQ also uses global gridded soil information based on the 2019 SoilGrids<sup>TM</sup> 250 m resolution data (<https://www.isric.org/explore/soilgrids>, last access: 5 April 2022) to drive an inline FENGSHA windblown dust model (Fu et al., 2014; Huang et al., 2015; Dong et al., 2016) in NACC-CMAQ (Fig. 2). Section 2.2 below provides more information on the specific parameters used in FENGSHA.

As in the prior NAQFC, the chemical initial conditions (beginning on 20 July 2021 for NACC-CMAQ) are taken from the previous day's (CMAQ) forecast output, and a NRT bias-correction using AirNow surface observations (<https://www.airnow.gov/>, last access: 5 April 2022) is applied to the 72 h predictions of O<sub>3</sub> and PM<sub>2.5</sub> (Fig. 2). Huang et al. (2017) provides more information on the bias-correction technique.

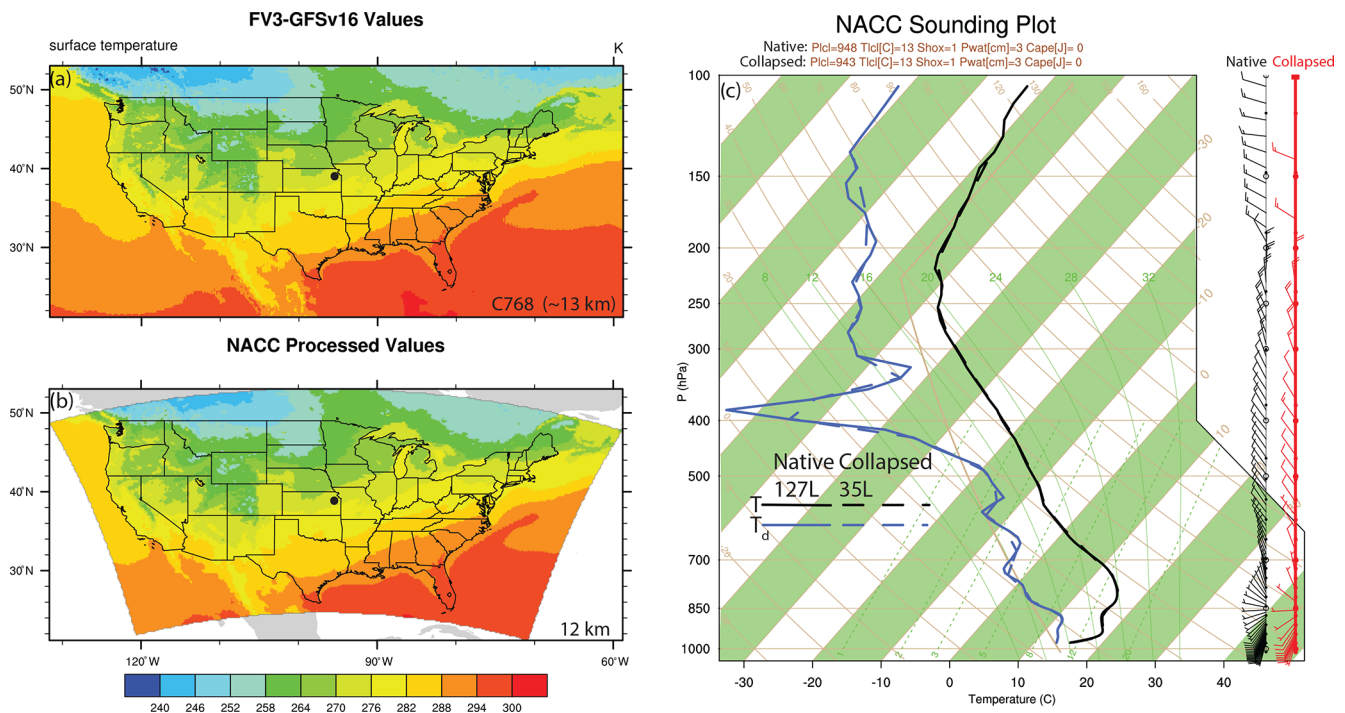


**Figure 3.** Examples of the NACC-CMAQ (a) GFSv16 Gaussian grid surface temperature (C768 ~ 13 km), (b) associated bilinear horizontal interpolation NACC LCC output (12 km), and (c) Skew-T Log-P diagram of both native GFSv16 (127 layers; solid) and interpolated NACC (35 layers; dashed) profiles of temperature (black), dew point (blue), and wind speed and direction (wind barbs, with native shown in black and collapsed shown in red). The example sounding pertains to a date of 24 September 2020 at the closest model grid square to 39.07° N and 95.62° W (black dot in a–b).

## 2.2 Updated chemistry, emissions, and air–surface exchange processes

### 2.2.1 The Community Multiscale Air Quality (CMAQ) model version 5.3.1

A major update in NACC-CMAQ is coupling the GFSv16 to a state-of-the-science chemical transport model, CMAQv5.3.1 (US EPA, 2019; Appel et al., 2021) (Fig. 2). The prior NAQFC and experimental GFSv15-CMAQ both use CMAQv5.0.2, released in April 2014 (US EPA, 2014). The major release of CMAQv5.3 incorporates significant improvements to gas chemistry (e.g., halogen-mediated ozone loss), aerosol modules (e.g., improved secondary organic aerosol formation), photolysis rates, aqueous and heterogeneous chemistry, transport processes, air–surface exchange, emissions, and other structural and computational improvements (Appel et al., 2021). The use of CMAQv5.3.1 in NACC-CMAQ also contains a number of bug fixes to v5.3. Version 6 of the Carbon Bond (CB6) mechanism is used for gas-phase chemistry (Yarwood et al., 2010), and the updated US EPA’s AERO7 module is used for aerosol formation in NACC-CMAQ. The US EPA’s GitHub web page ([https://github.com/USEPA/CMAQ/blob/master/DOCS/Release\\_Notes/README.md](https://github.com/USEPA/CMAQ/blob/master/DOCS/Release_Notes/README.md), last access:

5 April 2022) contains the CMAQv5.3 and v5.3.1 release notes, mechanism descriptions, and enhancements.

### 2.2.2 National Emissions Inventory Collaborative (NEIC) 2016 version 1 emissions

The anthropogenic emissions modeling data may be the most influential input for chemical transport model predictions in any AQF system (Matthias et al., 2018). The model emissions are updated from National Emissions Inventory (NEI) 2014 version 2 (2014v2) that is used by the prior NAQFC to NEI Collaborative (NEIC) 2016 version 1 (2016v1) Emissions Modeling Platform (NEIC, 2019), which is based on updated models and datasets applied to the US Environmental Protection Agency’s (EPA) NEI2014v2. The prior NAQFC uses an older NEI2014v2 emissions dataset. There have been substantial updates to the NEIC2016v1, which include emission decreases for CO, NO<sub>x</sub>, SO<sub>2</sub>, and PM<sub>2.5</sub> and increases in total VOC and ammonia (NH<sub>3</sub>) emissions compared to NEI2014v2 (NEIC, 2019). The intermittent, “event-based” emissions from wildfires and windblown dust, as well as persistent biogenic emissions sources, are not from the NEIC2016v1 but are instead dynamically predicted inline within NACC-CMAQ (described in following sections). The NEIC2016v1 area source (i.e., 2-D) emissions are given in a gridded netCDF/IOAPI format that are interpolated to the

12 km NAQFC domain. The NEIC2016v1 also provides major point source (i.e., 3-D) emissions from six sectors: commercial marine vehicles (CMV12 and CMV3), electricity-generating units (EGUs), non-EGUs, oil–gas sources, and “other” point sources. The anthropogenic point source plume rise is calculated inline within NACC-CMAQ using the Briggs plume rise method (Briggs, 1965). Slight adjustments are made to reduce the anthropogenic aerosol and fugitive dust emissions over snow and wet soil surfaces to account for different forecasted meteorology in GFSv16 compared to the conditions used in generating the NEIC2016v1.

We note that the NEIC2016v1 emissions are not projected into the actual forecast year, with the time lag being a long-recognized issue in NAQFC (e.g., Tong et al., 2012). Thus, the NACC-CMAQ air quality simulations for the fall of 2020 and the winter of 2021 are impacted by the COVID-19 pandemic, which resulted in spatiotemporal changes to emission patterns and ozone formation over the US in 2020 and beyond (Campbell et al., 2021). In addition, mobile source emissions have continued to decline since 2016, and thus it is likely that the emissions used in the analysis do not entirely reflect recent changes to the emissions compared to 2016 (almost 5 years earlier). We are actively working to improve the representativeness of anthropogenic emissions sources in NACC-CMAQ and next-generation versions of the NAQFC.

### 2.2.3 Inline biogenic emissions and bidirectional NH<sub>3</sub> fluxes

NACC-CMAQ uses the latest version of the Biogenic Emission Inventory System (BEIS) v3.6.1 (Vukovich and Pierce, 2002; Schwede, 2005) for estimating the biogenic VOC (BVOC) emissions. BEISv3.6.1 includes updated vegetation inputs and advanced two-layer canopy model formulations for estimating leaf (sun and shade) temperatures and vegetation data (Weiss and Norman, 1985; Campbell and Norman, 1998; Niinemets et al., 2010; Bash et al., 2016). NACC-CMAQ also uses the revised Biogenic Emissions Landuse Dataset version 5 (BELD5), which includes a newer version of the Forest Inventory and Analysis (FIA) version 8.0 and updated agricultural land use from the 2017 US Department of Agriculture (USDA) crop data layer. The BELD5 dataset also uses a MODIS 21-category land use dataset with lakes identified separately from oceans. The prior NAQFC used a much older BELD3 version (<https://www.epa.gov/air-emissions-modeling/biogenic-emissions-landuse-database-version-3-beld3>, last access: 6 April 2022).

The prior NAQFC also only considered summer factors in BEIS and did not capture seasonal (summer and winter) changes to the normalized biogenic emissions factors (specific to vegetation species). NACC-CMAQ is improved and uses a new “vegetation frost switch” that adjusts between summer and winter normalized emission factors in BEISv3.6.1 based on the calendar date and 2 m temperature

(TEMP2). In NACC, a new time-dependent variable, “SEASON” is equal to 1 during the growing season or equal to 0 outside the growing season. The SEASON is (boreal) summer if the calendar date is on or between 15 April and 15 October but switches to winter if TEMP2 drops below 28 °F (−2 °C), and it is winter if the date is on or between 16 October and 14 April but switches to summer if TEMP2 rises above 32 °F (0 °C). Thus, the SEASON variable in NACC-CMAQ differs from typical retrospective CMAQ applications and is more dynamic with hourly variability based on the GFSv16-forecasted TEMP2. Test results show generally improved model performance for all US regions in December 2020 (winter) with vegetation frost switch compared to using only summer season normalized emissions (Table S1 in the Supplement). Using BELD5 further improves model performance and reduces the error in all CONUS regions compared to the older BELD3 used in December 2020 tests (Table S1).

NACC-CMAQ includes bidirectional NH<sub>3</sub> (BIDI-NH<sub>3</sub>) for NH<sub>3</sub> fluxes (i.e., both deposition and evasion) in the CMAQv5.3.1 “M3Dry” deposition model (Nemitz et al., 2000; Cooter et al., 2010; Massad et al., 2010; Pleim and Ran, 2011; Bash et al., 2010, 2013; Pleim et al., 2013; 2019). Here, the NH<sub>3</sub> fertilizer emissions are removed from the base NEIC2016v1 inventory to avoid double counting, as the inline BIDI-NH<sub>3</sub> module calculates these fluxes. The BIDI-NH<sub>3</sub> module typically requires daily inputs (e.g., soil ammonia content, soil pH, soil moisture, and other soil characteristics) from the USDA’s Environmental Policy Integrated Climate (EPIC) agroecosystem model (<https://epicapex.tamu.edu/epic/>, last access: 5 April 2022; Williams et al., 1995) to calculate the soil ammonia concentrations that are combined with air concentrations in CMAQ to calculate BIDI-NH<sub>3</sub> fluxes. Typically, the Fertilizer Emission Scenario Tool (FEST-C, <https://www.cmascenter.org/fest-c/>, last access: 5 April 2022) processes the necessary meteorological conditions for integration with the EPIC simulation for input to CMAQ (Ran et al., 2011; Cooter et al., 2012). Use of the EPIC/FEST-C system is not feasible in an NRT operational forecasting model, and thus we use a pre-generated, full-year 2011 EPIC/FEST-C simulation based on Campbell et al. (2019) for the daily inputs to BIDI-NH<sub>3</sub> in NACC-CMAQ. NACC-CMAQ directly uses the GFSv16 soil moisture conditions in place of the FEST-C processed soil conditions required for the latest version of BIDI-NH<sub>3</sub> in CMAQv5.3.1 (Pleim et al., 2019).

### 2.2.4 Inline wildfire smoke and windblown dust emissions

Wildfires have been increasing in size (Westerling et al., 2006) and potentially in severity (Miller et al., 2009) over the past decades. Wildfire smoke outbreaks can lead to extreme concentrations of PM<sub>2.5</sub> and enhanced O<sub>3</sub> and are major concerns for air quality forecasting and consequential hu-

man and ecosystem health impacts. NACC-CMAQ includes a new inline calculation of wildfire smoke emissions based on the Blended Global Biomass Burning Emissions Product (GBBEPx V3; Zhang et al., 2012, 2014). GBBEPx provides daily global biomass burning emissions (PM<sub>2.5</sub>; black carbon, BC; organic carbon, OC; NO<sub>x</sub>; NH<sub>3</sub>; CO; and SO<sub>2</sub>). It blends fire observations from two sensors, including the Moderate Resolution Imaging Spectroradiometer (MODIS) on the NASA Terra and Aqua satellites and the Visible Infrared Imaging Spectrometer (VIIRS) on the Suomi National Polar-orbiting Partnership (SNPP) and Joint Polar-orbiting Satellite System 1 (JPSS1) satellites. The GBBEPx data are further processed to prepare model-ready emission datasets. First, the 0.1 × 0.1° latitude and longitude data are converted into the NAQFC LCC projection. US EPA-based Sparse Matrix Operator Kernel Emissions (SMOKE) fire speciation and diurnal profiles provide the PM speciation and diurnal patterns in NACC-CMAQ, respectively, while both land use and region are used to identify fire types. The fire duration persists for the 72 h forecast period (with scaling of 1.0, 0.25, and 0.25 for day 1, 2, and 3, respectively) for wildfires identified when the grid cell forest fraction is > 0.4. In the eastern US (longitude east of 100° W), however, the fires are assumed to be mainly prescribed burns in forested regions that only persist for the first 24 h. The wildfire plume rise is calculated inline within NACC-CMAQ using either the Briggs (1965) or Sofiev et al. (2012) algorithms (Wilkins et al., 2019); currently the Briggs method is used by default.

Climate models project warming and drying trends in the southwestern US, where intermittent windblown dust storms are becoming more frequent with the occurrence of drought (Tong et al., 2017) or even “megadrought” conditions (Williams et al., 2020). Windblown dust storms can lead to extreme levels of coarse-mode particulate matter (i.e., PM<sub>10</sub>) and cause detrimental effects to human and agroecosystem health and visibility. NACC-CMAQ includes a novel inline methodology for calculating windblown dust based on the FENGSHA model (Huang et al., 2015; Dong et al., 2016). In NACC-CMAQ, the potential for vertical dust flux in FENGSHA is generally controlled by the sediment supply map (SSM), and the magnitude of the friction velocity (USTAR) compared to a threshold friction velocity (UTHR) that determines the USTAR needed to transfer dust from soil surfaces to the atmosphere. The UTHR is dependent on the land cover, soil type, and soil moisture. The SoilGrids™ 250 m high-resolution dataset (<https://www.isric.org/explore/soilgrids>, last access: 5 April 2022) provides the necessary clay, silt, and sand fractions used to calculate the SSM.

### 2.3 Updated dynamic aerosol boundary conditions

The chemical lateral boundary conditions (CLBCs) are critical to the prediction accuracy of regional chemical transport models, particularly during intrusion events (Tang

et al., 2009, 2021). The CLBCs represent the spatiotemporal distribution of chemical species along the lateral boundaries of the domain of a regional model. NACC-CMAQ uses methods described in Tang et al. (2021) and implements dynamic CLBCs (updated every 6 h) for dust and smoke aerosol data that are extracted (and mapped to CMAQ CB6-Aero7 species) from the NOAA operational global atmospheric aerosol model, known as the Global Ensemble Forecast-Aerosols (GEFS-Aerosols) member (Fig. 2). GEFS-Aerosols is also based on the FV3GFS dynamical core, which uses the Goddard Chemistry Aerosol Radiation and Transport (GOCART) model for its sulfate, dust, BC, OC, and sea salt aerosol predictions (Chin et al., 2000, 2002; Ginoux et al., 2001). GEFS-Aerosols uses the same wildfire smoke and windblown dust dataset and algorithms as in NACC-CMAQ. The operational version of GEFS-Aerosols is run by the NWS as a special unperturbed forecast of the Global Ensemble Forecast System version 12 (<https://www.ncdc.noaa.gov/data-access/model-data/model-datasets/global-ensemble-forecast-system-gefs>, last access: 5 April 2022), which provides an ensemble forecast product four times per day. Dynamic CLBCs capture the signals of aerosol intrusion events such as biomass burning or windblown dust plumes from outside the domain, which can improve the prediction accuracy of downstream O<sub>3</sub> and PM<sub>2.5</sub> concentrations at the surface (Tang et al., 2021).

### 3 Simulation design and evaluation protocol

Table 1 summarizes the GFSv16 and NACC-CMAQv5.3.1 model configuration described in Sect. 2, as well as some additional model details. The model components and configurations used in prior NAQFC system are summarized in Table S2 (based on Lee et al., 2017) for comparison.

The simulation design consists of evaluations of continuous 1-month NACC-CMAQ (72 h, 3 d forecast) and prior NAQFC (48 h, 2 d forecast) simulations for September 2020 (late summer–fall period) and January 2021 (winter period) (with a previous 1-month spin-up and training data period) over the CONUS at a horizontal grid spacing of 12 km (Table 1). September 2020 is used for the warm season because it is the closest month to summer when both the NACC-CMAQ and prior operational NAQFC systems were simultaneously run. The prior operational NAQFC was discontinued on 20 July 2021 due to computational constraints at NWS/NOAA.

The Surface Weather Observations and Reports for Aviation Routine Weather Reports (METAR), collected by NCEP’s Meteorological Assimilation Data Ingest System (MADIS) ([https://madis.ncep.noaa.gov/madis\\_metar.shtml](https://madis.ncep.noaa.gov/madis_metar.shtml), last access: 5 April 2022), provide observations of TEMP2, 2 m specific humidity (Q2), and 10 m wind speed (WSPD10). The World Radiation Monitoring Center’s (WRMC’s) Baseline Solar Radiation Network (BSRN) (<https://bsrn.awi.de/>,

**Table 1.** GFSv16 and NACC-CMAQv5.3.1 model components and configurations. The abbreviation n/a stands for not applicable in this table.

Model attribute	Configuration	Reference
Domain	Conterminous US; Centered on 40° N, 97° W	n/a
Horizontal resolution	12 km	n/a
Vertical resolution	35 Layers from near the surface to about 14 km (~ 60 hPa)	n/a
Meteorological initial and boundary conditions	FV3GFSv 16	<a href="https://nws.weather.gov/">https://nws.weather.gov/</a> (last access: 5 April 2022)
Chemical ICs and BCs	2006 GEOS-Chem simulation & GEFS-Aerosol dynamic smoke and dust aerosol CLBCs	<a href="http://acmg.seas.harvard.edu/geos/">http://acmg.seas.harvard.edu/geos/</a> (last access: 5 April 2022) Tang et al. (2021)
Anthropogenic emissions	NEIC 2016v1 platform	NEIC (2019)
Biogenic emissions	Inline BEISv3.6.1 & BELD5	Vukovich and Pierce (2002); Schwede et al. (2005)
Wildfire emissions and plume rise	GBBEPxv3/ inline Briggs	<a href="https://www.ospo.noaa.gov/Products/land/gbbepx">https://www.ospo.noaa.gov/Products/land/gbbepx</a> (last access: 5 April 2022); Briggs (1965)
Microphysics	GFDL six-category cloud microphysics scheme	Lin et al. (1983); Lord et al. (1984); Krueger et al. (1995); Chen and Lin (2011, 2013)
PBL physics scheme	sa-TKE-EDMF	Han and Bretherton (2019)
Shallow and deep cumulus parameterization	SAS scheme	Han and Pan (2011); Han et al. (2017)
Shortwave and longwave Radiation	RRTMg	Mlawer et al. (1997); Clough et al. (2005); Iacono et al. (2008)
Land surface model	Noah land surface model	Chen and Dudhia (2001); Ek et al. (2003); Tewari et al. (2004)
Surface layer	Monin–Obukhov	Monin and Obukhov (1954); Grell et al. (1994); Jimenez et al. (2012)
Gas-phase chemistry	CB6	Yarwood et al., 2010
Aqueous-phase chemistry	CMAQ AQChem updates	Martin and Good (1991); Alexander et al. (2009); Sarwar et al. (2011)
Aerosol module and size	AERO7	Appel et al. (2021)
Other model attributes	– Inline photolysis – Inline bi-directional NH <sub>3</sub> exchange  – Inline FENGSHA windblown dust emissions – Inline sea salt emissions	Binkowski et al. (2007) Nemitz et al. (2000); Cooter et al. (2010); Massad et al. (2010); Pleim and Ran (2011); Bash et al. (2010, 2013); Pleim et al. (2013, 2019) Fu et al. (2014); Huang et al. (2015); Dong et al. (2016) Kelly et al. (2010); Gantt et al. (2015)

last access: 5 April 2022; Driemel et al., 2018) and US Surface Radiation Network (SURFRAD; <https://gml.noaa.gov/grad/surfrad/>, last access: 5 April 2022) provide shortwave radiation observations at the ground (SWDOWN). The PRISM Climate Group, Northwest Alliance for Computational Science and Engineering, at Oregon State University (<https://prism.oregonstate.edu/>, last access: 5 May 2021) provide gridded total precipitation observations (PRECIP). The National Oceanic and Atmospheric Administration

(NOAA) Earth System Research Laboratory's (ESRL's) Radiosonde Database (RAOB) (<https://ruc.noaa.gov/raobs/>, last access: 5 April 2022) provides vertical profile observations of temperature, relative humidity, and wind speed. The US EPA Air Quality System (AQS; <https://www.epa.gov/aqs>, last access: 5 April 2022) and near-real-time AirNow observational networks (<https://www.airnow.gov/>, last access: 5 April 2022) provide near-surface O<sub>3</sub> and PM<sub>2.5</sub> measurements.

The statistical measures used to evaluate the meteorological–chemical coupling and air quality predictions include the mean bias (MB), normalized mean bias (NMB), normalized mean error (NME), root-mean-square error (RMSE), anomaly correlation coefficient (ACC), Pearson's correlation coefficient ( $R$ ), and index of agreement (IOA). Statistical measures such as  $R$ , NMB, and NME provide measures of the associativity (i.e., correlation), bias, and accuracy, respectively, of specific modeled surface and vertical meteorology and surface  $O_3$  and  $PM_{2.5}$ . The meteorological and chemical evaluations use the publicly available US EPA Atmospheric Model Evaluation Tool (AMET; Appel et al., 2011) and NOAA/ARL Model and Observation Evaluation Toolkit (MONET; Baker et al., 2017).

## 4 Results

### 4.1 Meteorological analysis

Compared to NMMB used in the prior NAQFC, the GFSv16 model has lower actual TEMP2 in the east and southeast and parts of the northwest (Fig. 4a–d) but has higher TEMP2 in the central Great Plains, northern Great Plains, and parts of the western and southwestern US, with higher 10 m wind speeds (WSPD10) in these regions (Fig. 4i–l). GFSv16 is drier with widespread lower 2 m specific humidity (Q2; Fig. 4e–h) and lower cloud fractions (CFRAC) (Fig. 4m–p), higher solar radiation absorbed at the ground (GSW; Fig. 5a–d), lower longwave radiation absorbed at the ground (GLW; Fig. 5e–h), deeper planetary boundary layer height (PBLH; Fig. 5i–l), and generally more regions of increased precipitation (PRECIP; Fig. 5m–p). Differences in the CFRAC are (in part) impacted by differences in the model definition of cloud cover; NMMB uses a binary cloud cover definition at each grid point, while GFSv16 uses fractional cloud cover to calculate CFRAC. For stable conditions, the PBLH in the prior NAQFC is re-diagnosed based on the Troen and Mahrt (1986) incremental calculation of the bulk Richardson number ( $Ri_b$ ) from the surface up to a height above the neutral buoyancy level (i.e., approaching the critical Richardson number,  $Ri_{crit}$ ) in the Asymmetric Convective Model v2 (ACM2) PBL scheme in CMAQ (Pleim 2007a, b). For unstable conditions, the re-diagnosed ACM2 uses a slightly different PBLH formulation based on first finding the convectively unstable mixing layer ( $z_{mix}$ ) and then defining the point where  $Ri_b = Ri_{crit}$  for the entrainment layer above  $z_{mix}$ . For both stable and unstable conditions, however, NACC-CMAQ directly uses the diagnosed PBLH from the turbulent kinetic energy (TKE)-based PBL scheme in GFSv16 (Table 1; Han and Bretherton, 2019), which is also based on the Troen and Mahrt (1986) incremental  $Ri_b$  formulation. Thus, NACC/GFSv16-CMAQ calculation is similar to the re-diagnosed ACM2 PBLH for nighttime-stable conditions

(with slight differences in  $Ri_{crit}$  values), while there exists some distinct differences in their daytime-unstable PBLH formulations and  $Ri_{crit}$  calculations.

Consequently, the GFSv16 (NACC) and re-diagnosed ACM2 (prior NAQFC) diurnal PBLH patterns are similar at night; however, the GFSv16 PBLH is considerably higher than the prior NAQFC during the daytime for all regions in September and January (Figs. S4–S5).

The meteorological differences between GFSv16 and NMMB (Figs. 4–5) influence chemical predictions in CMAQ, which include a deeper daytime PBL and more precipitation that can effectively dilute the gaseous and aerosol concentrations for NACC-CMAQ in some regions across the CONUS. Areas of lower CFRAC and higher TEMP2 in GFSv16, however, will increase photolysis and daytime  $O_3$  formation in NACC-CMAQ in certain regions including the southern US and upper Great Plains. We note that although there are differences in the PBLH calculation methodologies between the prior NAQFC and NACC-CMAQ (particularly for the unstable daytime PBLH), the differences in near-surface meteorology (i.e., generally warmer and drier) conditions in the GFSv16 (Tables 2 and S2) also in part affect the differences in PBLH (Fig. 5i–l). These differences affect the pollutant mixing and dilution, and in part the resulting air quality predictions between the prior NAQFC and NACC-CMAQ (see Sect. 4.4 below).

### 4.2 Meteorological evaluation and metrics

Evaluation of the simulated day 1 (0–24 h) forecasted meteorology against the METAR network shows that GFSv16 generally has a higher positive TEMP2 (warmer) bias (Fig. 6) in the west and a CONUS-wide higher negative Q2 (dry) bias (Fig. 7) compared to prior NMMB (i.e., prior NAQFC) in both September and January.

There are regions of higher RMSE for T2 and Q2, and lower and degraded ACC (Figs. S7–S8) for GFSv16 compared to NMMB, especially in the southern and western CONUS regions during September. The spatial patterns and magnitudes of WSPD10 bias and error are similar between GFSv16 and NMMB (Fig. 8); however, the higher WSPD10 for GFSv16 in the southern and central CONUS leads to a shift from negative to positive biases from Texas northward to North Dakota, especially during September. The WSPD10 RMSE is higher (Fig. 8) and the ACC is also lower/degraded (Fig. S9) for GFSv16 in those regions, but otherwise the GFSv16 and NMMB have similar performance for WSPD10. The day 1 forecast model performance (MB, RMSE, and ACC) for 10 m wind direction (WDIR10) is similar between NMMB and GFSv16 in both September and January (Figs. S6 and S10).

Overall, the GFSv16 results are favorable for driving the advanced NACC-CMAQ system, with some areas of concern in the degraded TEMP2 and Q2 in the warmer and drier regions, particularly in the south and west CONUS during



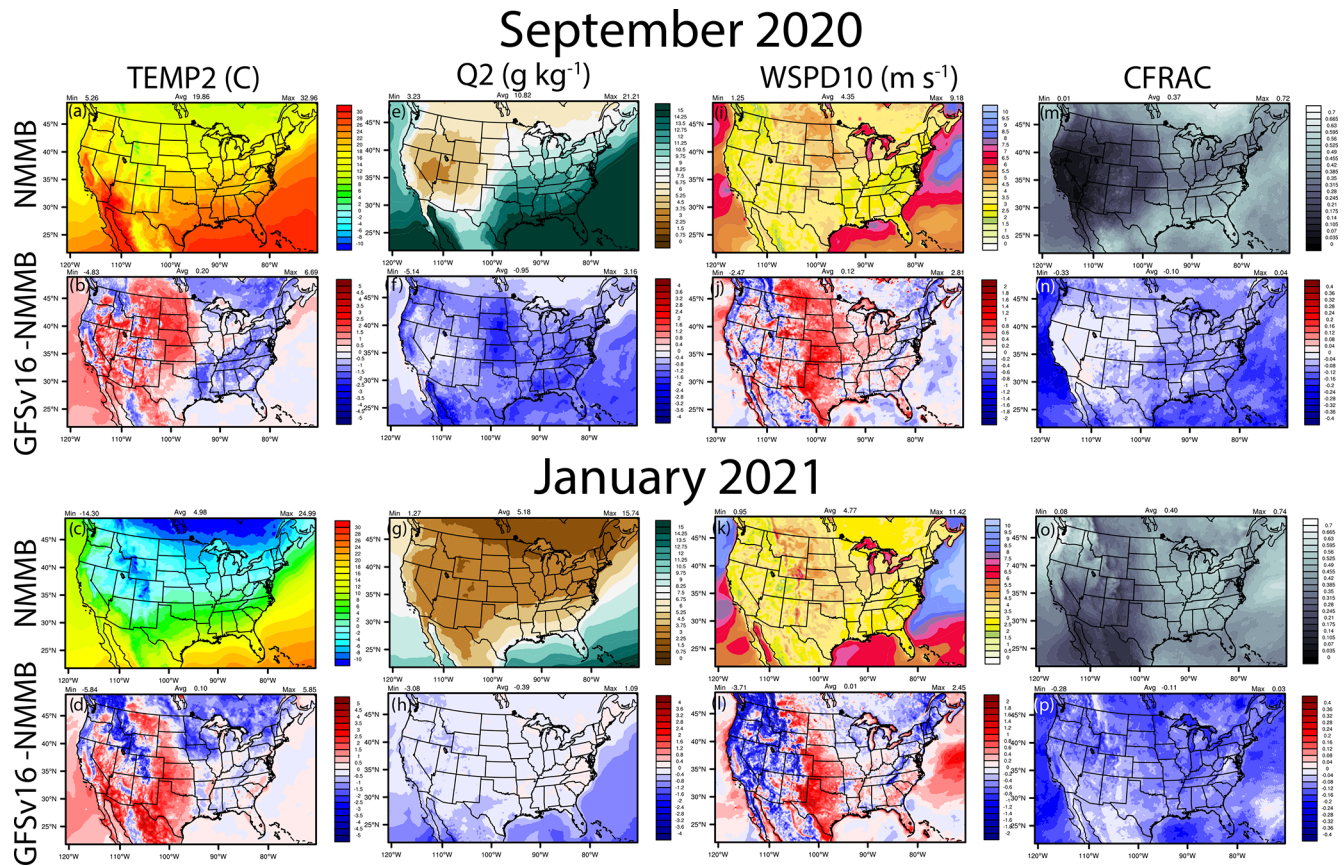


**Figure 4.** September 2020 and January 2021 spatial average plots for NMMB (prior NAQFC) and the absolute differences for GFSv16 (NACC) – NMMB for TEMP2, Q2, WSPD10 and CFRAC.

September. This roughly correlates with warmer/drier top-layer soil conditions in GFSv16 in these regions (Fig. S11), and thus land surface and soil data assimilation and model improvement in GFSv16 is an active area of focus at NOAA. The widespread dry bias in GFSv16 appears to be persistent, as an independent evaluation of August 2019 demonstrated a very similar spatial pattern and magnitude of Q2 under-predictions in the eastern half of CONUS compared to the METAR network (not shown).

The GFSv16-driven NACC-CMAQ system extends out to a 72 h forecast. Hence, there is a question of how the day 1 and 2 forecasts perform for NMMB vs. GFSv16 in the eastern (< 100° W) and western (> 100° W) US and how a day 3 forecast extension also affects the GFSv16 diurnal and statistical model performance. The GFSv16/NACC diurnal patterns of standard deviation, error, and bias for TEMP2, Q2, and WSPD10 are very similar to each other for days 1–3 (Figs. S12–S14). While there is a slight increase in error and decreased correlation (*R*), the relevant statistical metrics (e.g., MB, NMB, RMSE, and *R*) do not change appreciably from day 1 to 3 for both September and January (Tables S3–S4). This lends confidence in the utility of using the updated

GFSv16 meteorology to drive a 72 h air quality forecast in NACC-CMAQ.

The day 1 diurnal statistics highlight both similar and contrasting TEMP2 and Q2 patterns for NMMB vs. GFSv16 in the eastern and western CONUS (Figs. S12–S13). In September (Fig. S12a), NMMB has higher error and positive TEMP2 (i.e., warm) bias in eastern CONUS during morning hours and lower error with a slight cool bias in the afternoon and evening, while GFSv16 shows slightly overpredicted TEMP2 during most hours of the day in the east. Over the western CONUS, there are larger diurnal TEMP2 differences that include small oscillating TEMP2 biases (about zero) for NMMB, along with distinctly large warm biases during all daytime hours for GFSv16 in the west. There are larger error and negative Q2 (i.e., drier) biases for GFSv16 compared to NMMB in eastern and western CONUS (Fig. S13a). In January, the TEMP2 and Q2 diurnal statistical patterns are similar for NMMB and GFSv16 in both the eastern and western CONUS; however, the GFSv16 daytime hours have slightly higher error and warmer and drier biases compared to NMMB (Figs. S12b and S13b).

The total PRECIP is generally higher in GFSv16 compared to NMMB toward the east (Fig. 5), which leads to



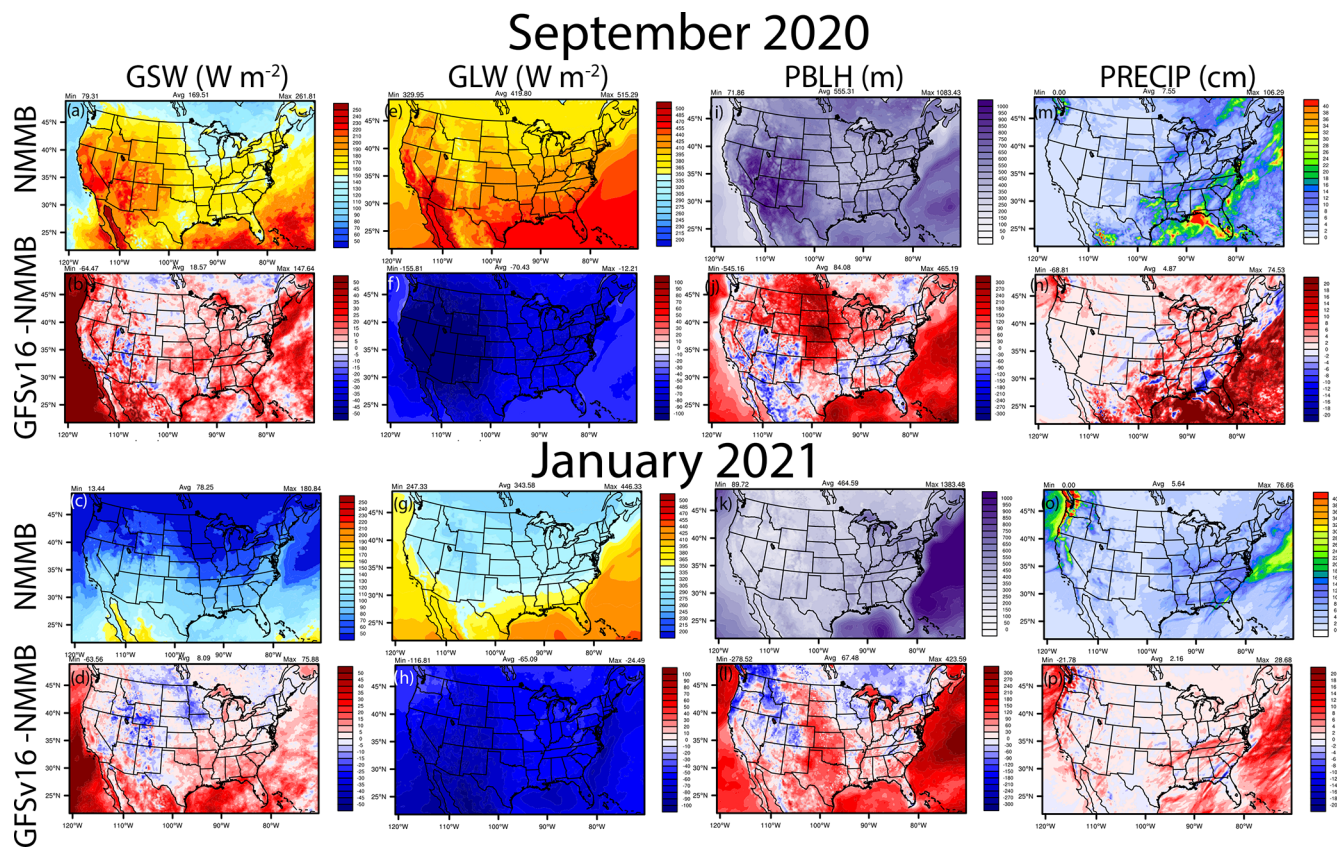


**Figure 5.** The same as Fig. 4 but for GSW, GLW, PBLH, and PRECIP.

larger overpredictions on average in the CONUS compared to PRISM (Fig. 9). GFSv16 has a positive PRECIP bias on average in the CONUS, NMMB has a negative bias, and there is a relatively large difference in the spatial patterns between NMMB and GFSv16 for September compared to January. The difference is impacted by higher convective activity during late summer and early fall in September compared to winter in January (not shown). Further analysis indicated that generally heavier PRECIP in GFSv16 reduces the predicted  $\text{PM}_{2.5}$  concentrations via wet deposition (not shown) in the east and southeast and in parts of the west and north-west compared to NMMB.

Comparisons of the model vertical profile statistics (i.e., MB, RMSE, and IOA) for TEMP, RH, and WSPD against an average of select RAOB observations across the CONUS indicate that the GFSv16 (NACC) performs consistently with the operational NMMB (NAQFC) column (Fig. 10; IOA nearly identical at  $\sim 0.8$ – $0.9$ ). GFSv16 is warmer and drier than NMMB in the model layers near the surface ( $> 850$  mb), especially in September; however, GFSv16 has a moister atmospheric column with higher wind speeds compared to NMMB above the surface and in the free troposphere ( $< 850$  mb). Figures S15–S17 show the spatial variability across the different RAOB sites used in the average for Fig. 10. Analysis of the column (1000–250 hPa) aver-

age for all CONUS RAOB sites across CONUS indicate that GFSv16 has a predominantly cooler and moister atmospheric column in September, despite being strongly warmer and drier near the surface (Figs. S18–S19).

### 4.3 Emissions analysis

The updated NEIC2016v1 emissions in NACC-CMAQ are lower compared to the NEI2014v2 emissions used in the operational NAQFC for all major species, except for  $\text{NH}_3$  (Table 2), as the NEI2016v1 includes updated data sources and model projections that have generally decreasing emissions compared to the NEI2014v2 (NEIC, 2019).

The spatial emission changes show widespread decreases in the 2-D area and mobile emissions near the major urban cities for CO and  $\text{NO}_x$  and across the major interstates and railways for  $\text{NO}_x$  (Fig. 11a–b).

The spatial variability in  $\text{NO}_x$  emission changes, however, are impacted by changes in a number of on-road inputs including vehicles miles traveled, age distribution, and speeds, which caused some emissions to go up or go down depending on the specific counties. The  $\text{NO}_x$  emissions variability is also impacted by national increases in railway levels and fuel use, while at the same time being impacted by changes to fuel efficiency and cleaner engines for both pas-

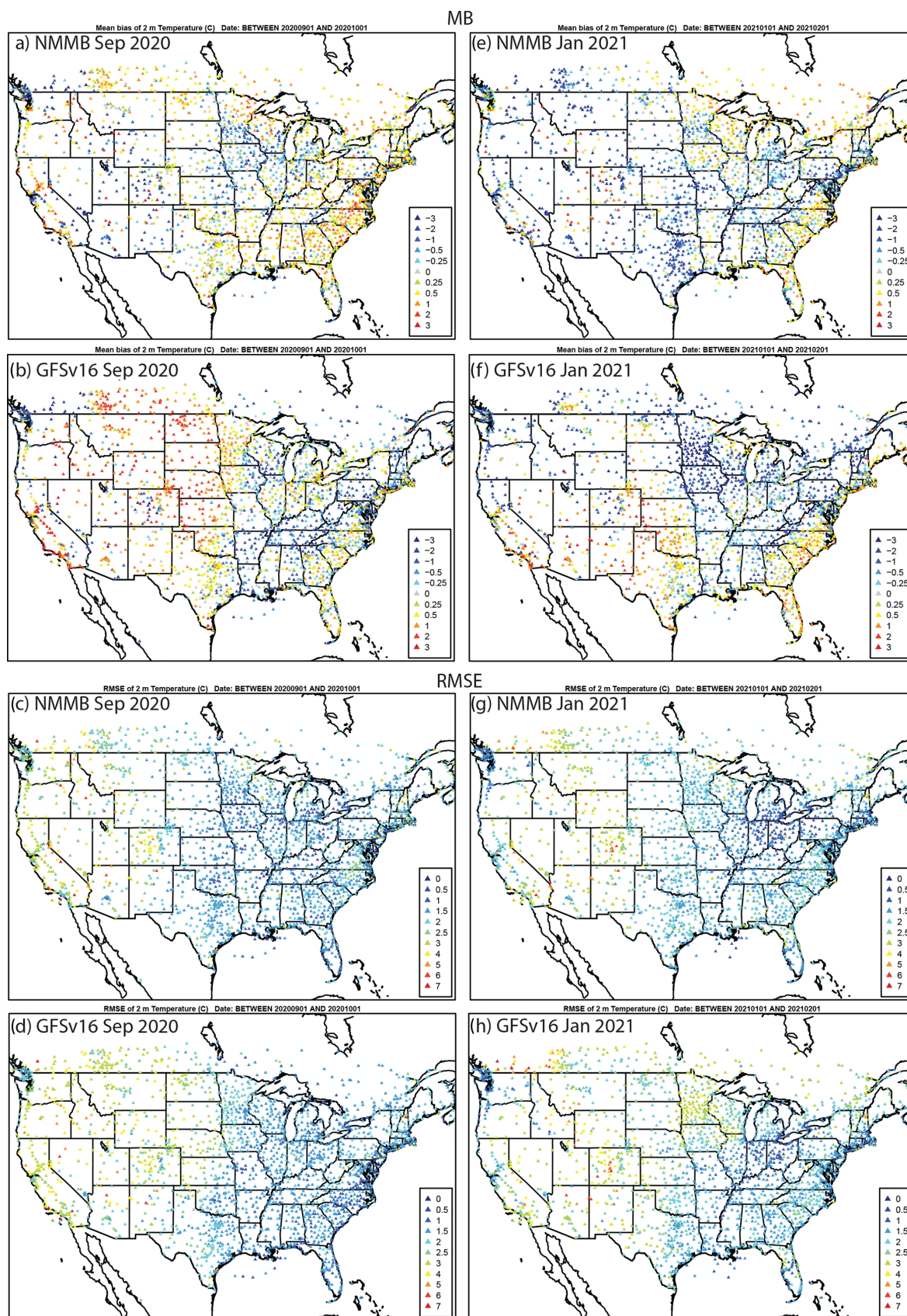


**Figure 6.** Average day 1 (0–24 h) forecasted TEMP2 MB (°C) and RMSE (°C) for NMMB and GFSv16 during (a)–(d) September 2020 and (e)–(h) January 2021 compared to METAR observations.



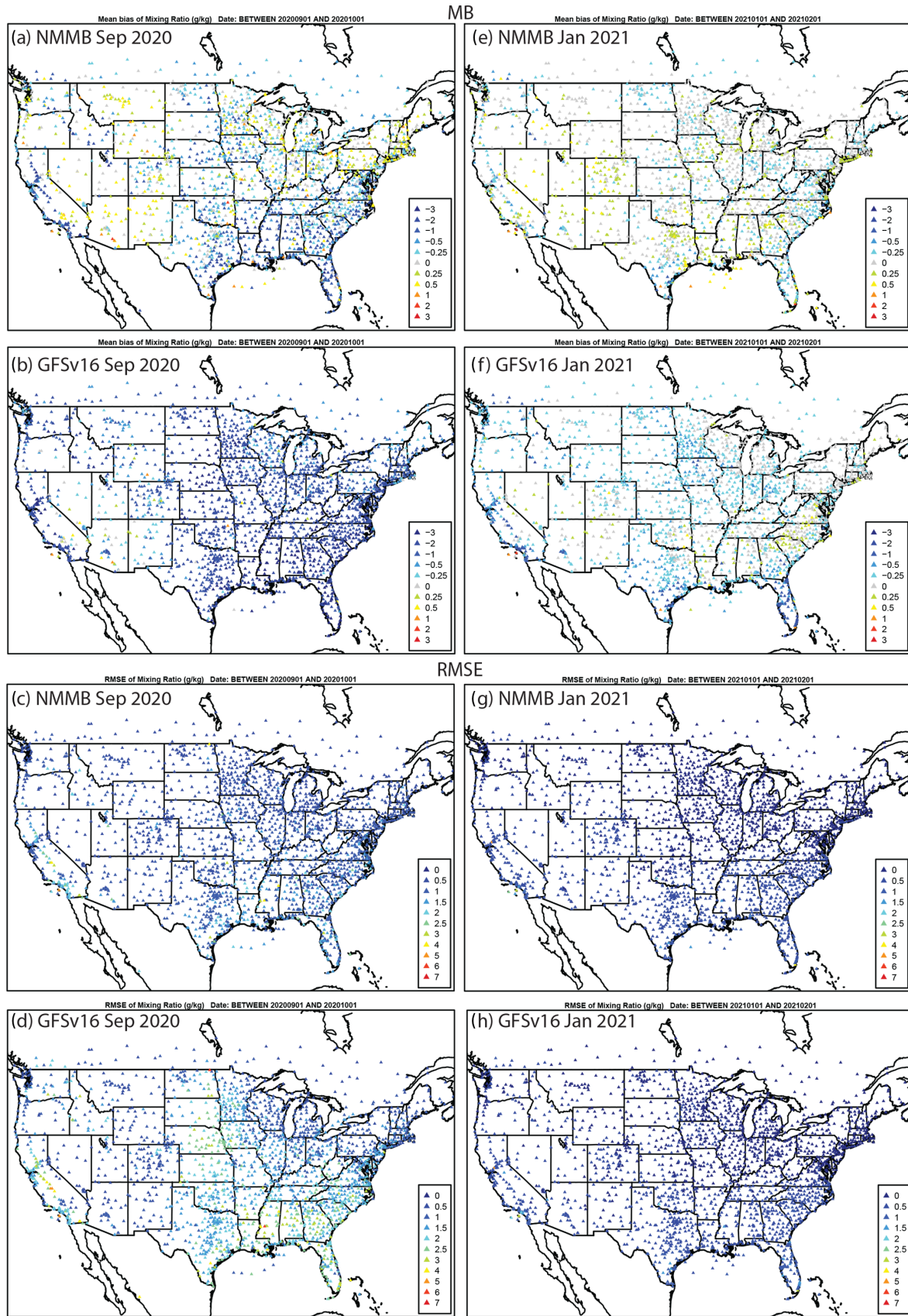


Figure 7. The same as Fig. 6 but for Q2 (g kg<sup>-1</sup>).

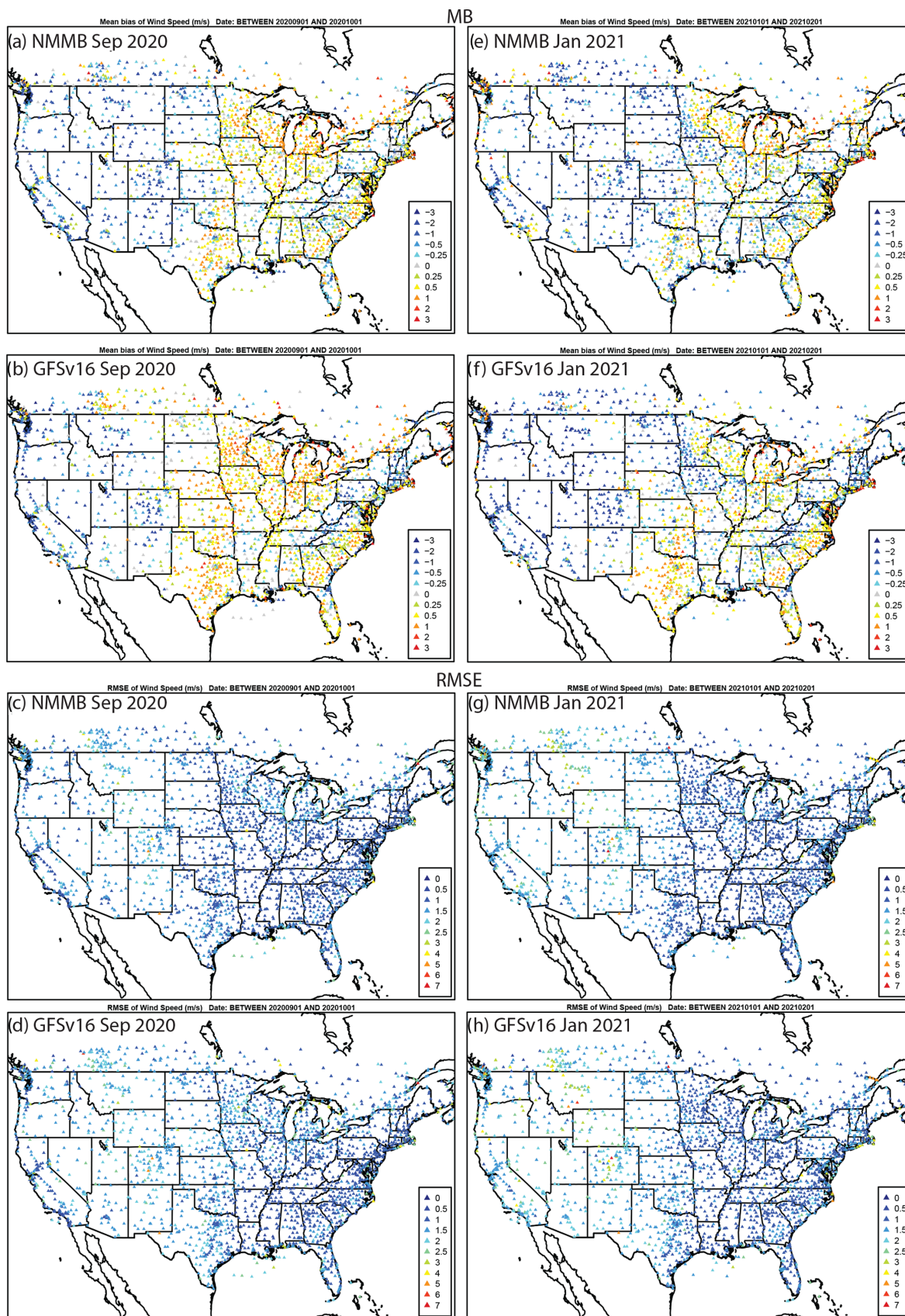
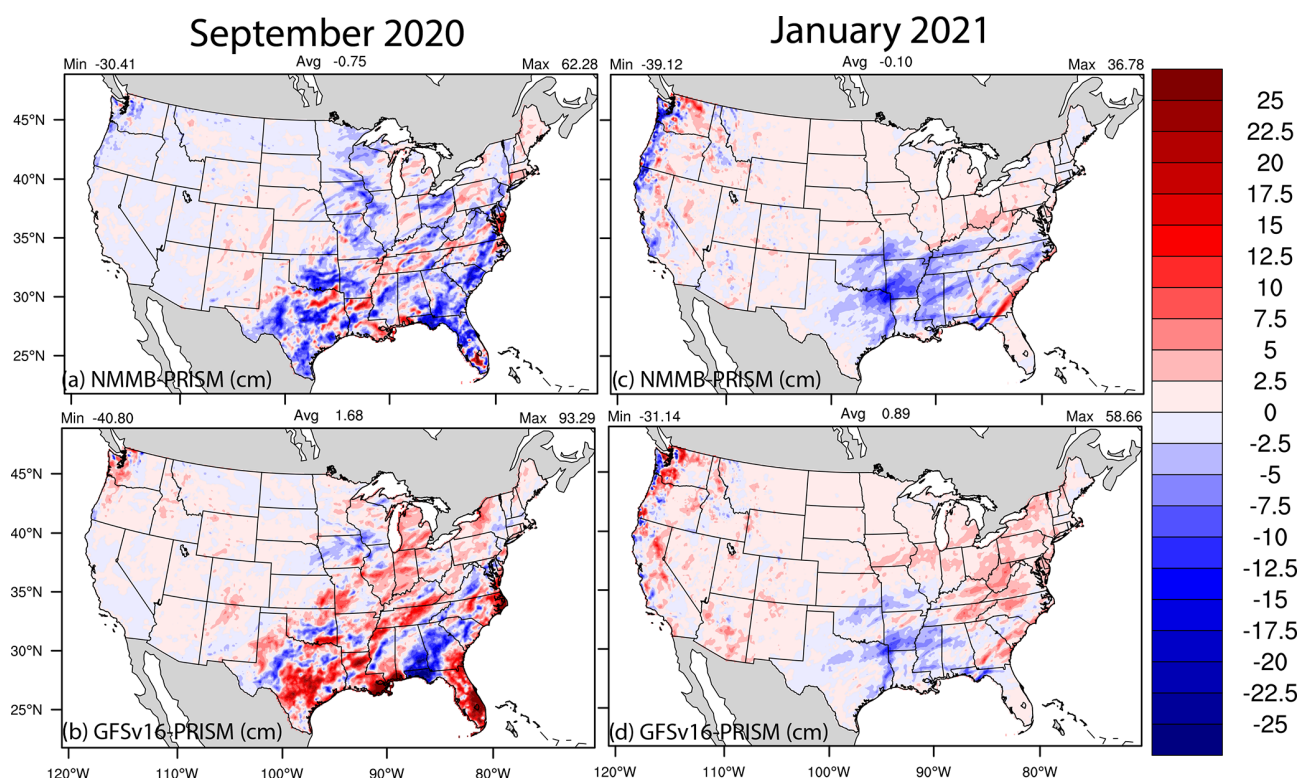


Figure 8. The same as in Fig. 6 but for WSPD10 ( $\text{m s}^{-1}$ ).





**Figure 9.** Average day 1 (0–24 h) forecasted total PRECIP (cm) biases (Predicted-PRISM) for NMMB (a, c) and GFSv16 (b, d) during (a)–(b) September 2020 and (c)–(d) January 2021.

**Table 2.** September and January emissions totals (Tg) for the NAQFC CONUS domain.

Emission species	NEI2014v2	NEIC2016v1	Percentage difference
September total (Tg)			
CO	4.69	4.27	−8.9
NO <sub>x</sub>	0.92	0.75	−18.1
SO <sub>2</sub>	0.54	0.37	−31.2
NH <sub>3</sub>	0.48	0.59	23.9
AVOC	215.58	195.60	−9.3
POC	0.07	0.05	−26.8
PEC	0.03	0.02	−23.9
PMC	2.03	0.82	−59.3
January total (Tg)			
CO	3.70	3.28	−11.2
NO <sub>x</sub>	0.78	0.64	−18.5
SO <sub>2</sub>	0.58	0.38	−34.7
NH <sub>3</sub>	0.10	0.12	18.4
AVOC	182.02	174.05	−4.4
POC	0.08	0.07	−10.8
PEC	0.02	0.02	−16.7
PMC	1.27	0.24	−80.8

senger and commuter trains. There are relatively minor area and mobile changes in SO<sub>2</sub> (Fig. 11c), with some exceptions in the east-northeast; however, there are widespread increases in NH<sub>3</sub> emissions driven by changes to the livestock counts and updated fertilization methods and inputs found in the NEIC2016v1 (Fig. 11d). Changes in non-point oil and gas production, exploration, and emission factors generation, as well as changes to updated activity and data sources for commercial cooking, residential fuel combustion, and industrial/commercial/institutional (ICI) fuel combustion impact the anthropogenic VOC (AVOC) area emission changes (Fig. 11e). The widespread and spatially consistent decreases in particulate organic carbon (carbon only)  $\leq 2.5 \mu\text{g}$  (POC) and PMC (defined as coarse PM  $> 2.5 \mu\text{g}$  and  $\leq 10 \mu\text{g}$ ) are due to decreasing fugitive dust sources (Fig. 11f and h), with the exception of the St. Lawrence River valley, that has both increases in POC and AVOC (e.g., formaldehyde; not shown) emissions in the NEIC2016v1. Updated appliance counts and residential wood combustion estimates affect the particulate elemental carbon  $\leq 2.5 \mu\text{g}$  (PEC) area emission decreases (Fig. 11g).

There are also biogenic emissions differences due to the updated inline BEISv3.6.1 and BELD5 in NACC-CMAQ (Table 2) and due to the impacts of NMMB (prior NAQFC) vs. GFSv16 (NACC) meteorology on BEIS calculations (Fig. 12).

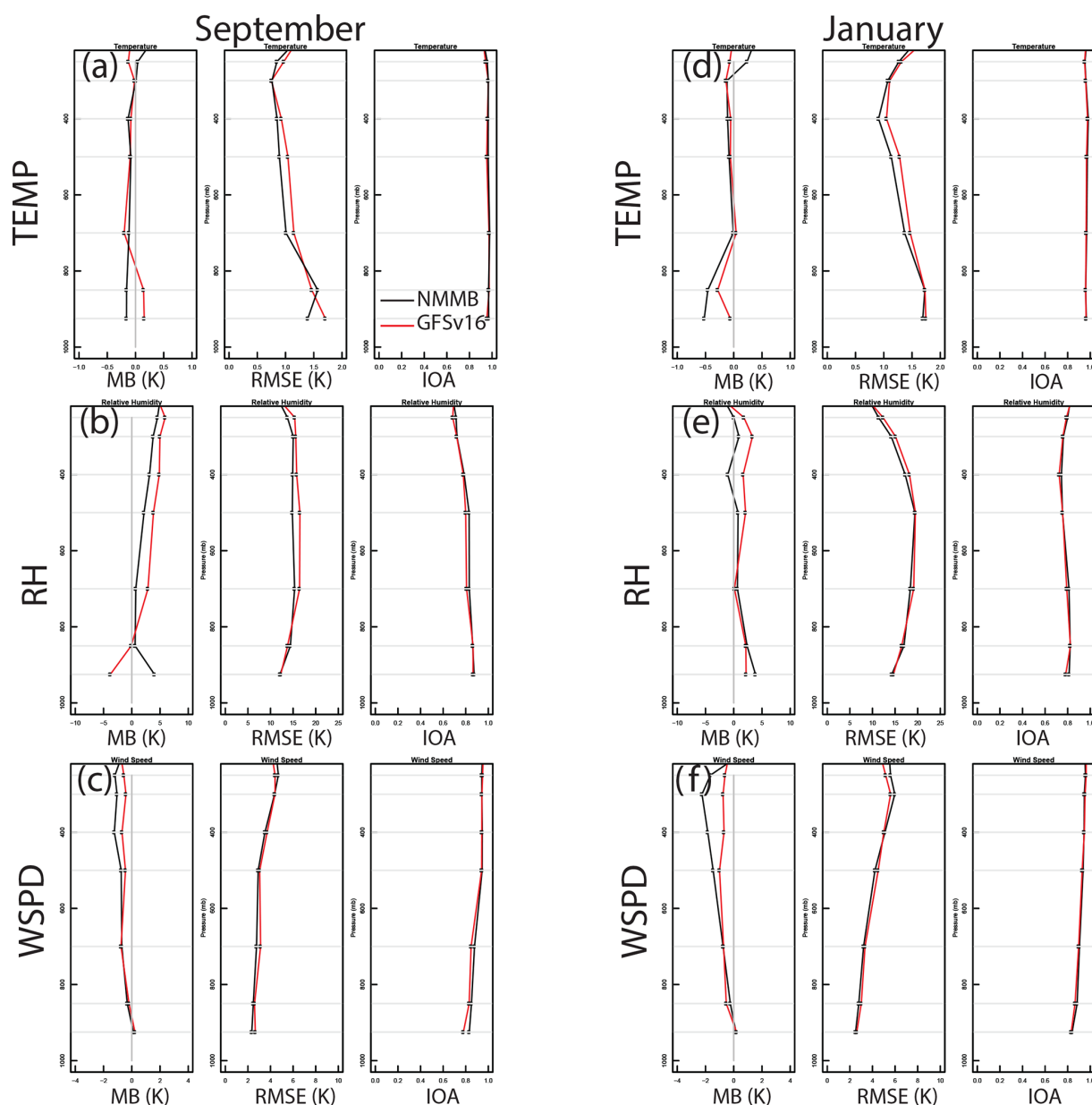


**Figure 10.** September 2020 (a, b, c) and January 2021 (d, e, f) vertical (1000–250 mb) temperature (TEMP), relative humidity (RH), and wind speed (WSPD) statistics (MB, RMSE, and IOA) for NMMB (black) and GFSv16 (red) against an average for select RAOB sites in the CONUS. Figure S15a shows the specific RAOB site profiles, and Figs. S18–S19 provide their relative locations.

The lower GFSv16 temperatures near many of the highly vegetated regions of the CONUS in September (Fig. 4b) decrease the isoprene (ISOP) and terpene (TERP) emissions, with some notable localized ISOP emission increases due to larger relative increases in downward solar radiation at the surface (GSW; Fig. 5b) and resulting photosynthetic active radiation (PAR; not shown). The differences are also impacted by the derivations of leaf temperatures in the updated BEISv3.6.1 and BELD5 in NACC-CMAQ compared to the BEISv3.14 and BELD3 in the prior NAQFC (see discussion in Sect. 2.2). Hence, the differences in spatial vari-

ability between ISOP and TERP emission changes stem from both differences in the locations of their relative maxima and from the different algorithms for temperature and light dependencies in BEIS. The GFSv16 (NACC) performs very similarly to NMMB (prior NAQFC) for GSW at the surface compared against BSRN-SURFRAD observations in the CONUS, with a slightly larger overprediction in the late afternoon at some sites (Figs. S21 and S22). The relatively low ISOP and TERP emissions in NACC-CMAQ will effectively lower the ground-level O<sub>3</sub> and contribution of secondary organic aerosol (SOA) formation to PM<sub>2.5</sub> compared to the

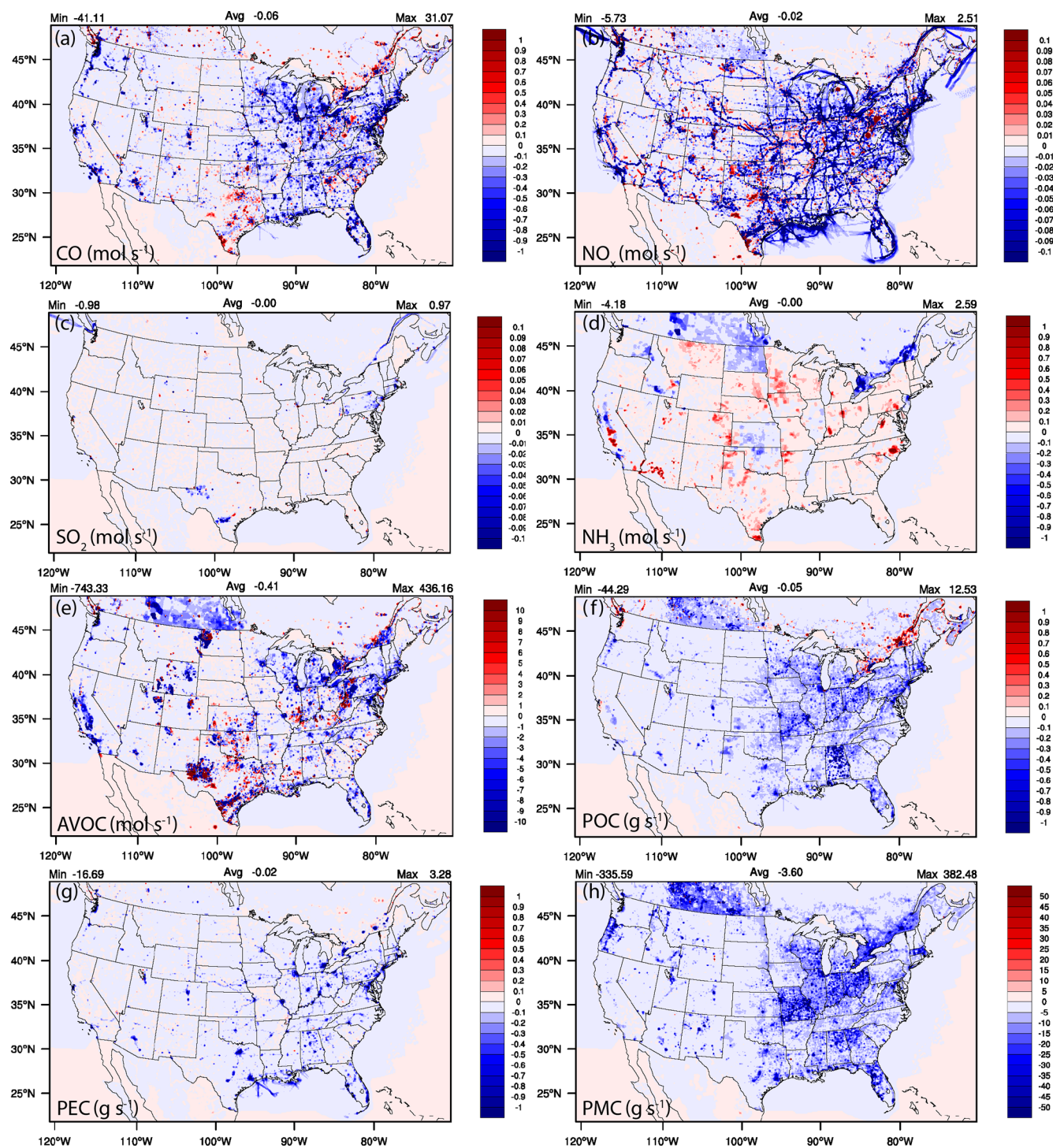


**Figure 11.** September 2020 average spatial difference plots for NEIC2016v1-NEI2014v2 combined 2-D area and mobile emissions. Figure S20 shows very similar emission changes for January 2021.

prior NAQFC, particularly in the southeast and parts of the western CONUS in the late summer and early fall.

#### 4.4 Air quality analysis

Here we focus on analysis of NACC-CMAQ predictions of gaseous O<sub>3</sub> for the late summer and early fall (September 2020) and PM<sub>2.5</sub> concentrations during the winter (Jan-



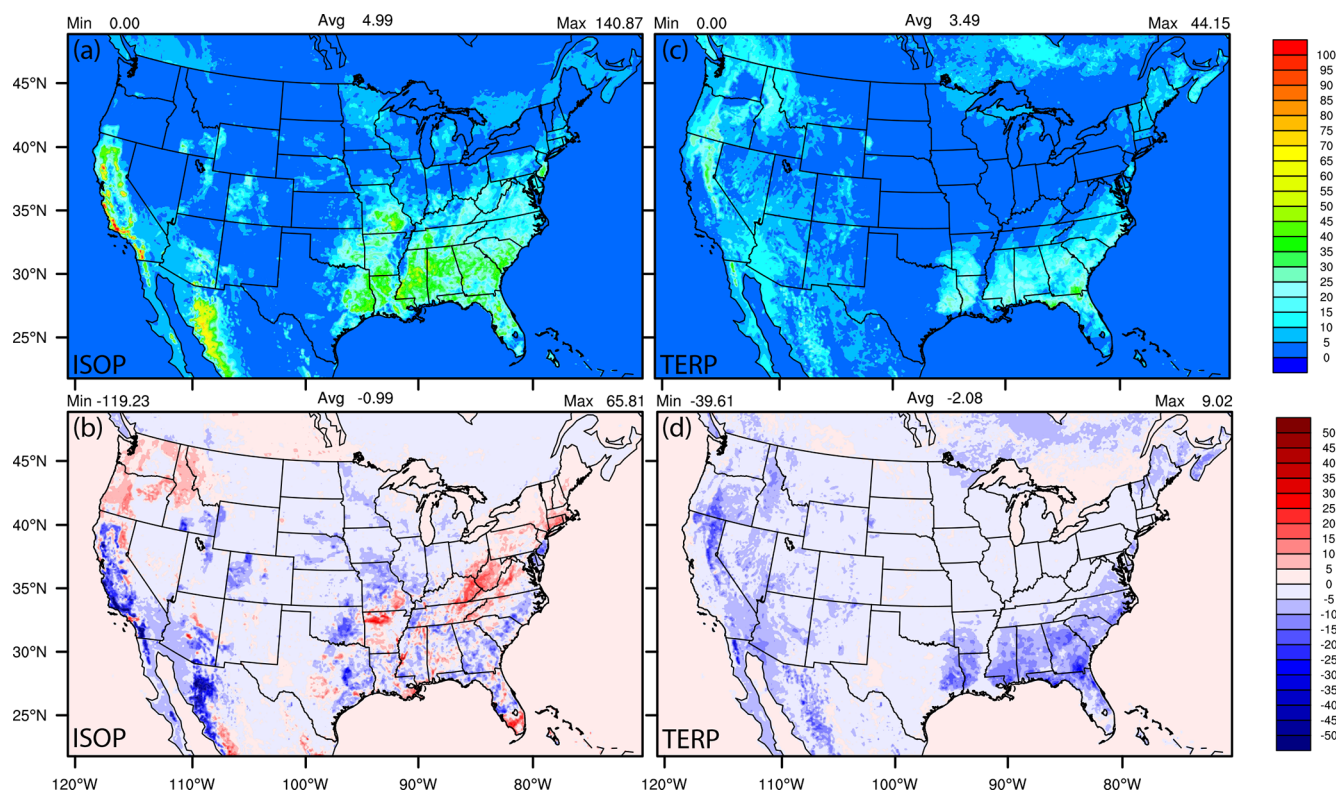


**Figure 12.** September 2020 average isoprene (ISOP) and terpene (TERP) emissions (a, b) in the prior NAQFC with BEISv3.1.4 and the absolute differences (c, d) between NACC-CMAQ (with BEISv3.6.1) and NAQFC.

uary 2021) as concentrations are relatively high for the pollutant's respective seasons. During the late US ozone season in September 2020, a large majority of the local  $\text{NO}_x$  concentration increases in NACC-CMAQ (Fig. 13a–b) correlate with areas of  $\text{NO}_x$  emissions increases in the NEIC2016v1 compared to the NEI2014v2 (Fig. 11b). An exception is the large  $\text{NO}_x$  increases in the far west (e.g., California and Oregon) that stem from gaseous  $\text{NO}_x$  emissions from strong wildfires that are captured by the GBBEPx in NACC-CMAQ (Table 1) but are excluded from the prior NAQFC wildfire emissions system (Table S2).

The increases in  $\text{NO}_x$  concentrations and enhanced nighttime  $\text{O}_3$  titration, widespread decreases in total VOC concentrations due to both anthropogenic and biogenic VOC emission decreases in NACC-CMAQ, GFSv16-meteorology impacts (e.g., higher PBLH), and updated CMAQv5.3.1 chemistry and transport lead to widespread decreases in hourly  $\text{O}_3$  when averaged over all hours (Fig. 13e–f). Regions of higher  $\text{NO}_x$  emissions, overall drier (i.e., widespread lower Q2) conditions, and stronger mid- to late-afternoon solar radiation reaching the surface (i.e., widespread lower CFRAC) (see Figs. 4–5 and S21–22) lead to enhanced daytime  $\text{O}_3$  formation, which is shown in the widespread increases in the maximum daily 8 h average (MDA8)  $\text{O}_3$  for NACC-CMAQ (Fig. 13g–h). This is particularly true for the strongly  $\text{NO}_x$ -limited conditions across much of the western CONUS,

where the MDA8  $\text{O}_3$  increases are impacted by large increases in wildfire  $\text{NO}_x$  emissions in GBBEPx and VOC decreases (anthropogenic+biogenic but no wildfire VOC emission impacts) in NACC-CMAQ. These effects subsequently impact the ozone  $\text{NO}_x$ -VOC sensitivity regime that enhances the  $\text{NO}_x$ -saturated (i.e., VOC-limited) conditions in this case (Fig. S24). There are exceptions, with MDA8  $\text{O}_3$  decreases in the west, including western Oregon, the San Joaquin Valley in California, and regions of the southwestern CONUS, all of which are strongly VOC-limited (Fig. S24). These regions are further impacted by the VOC decreases and further  $\text{NO}_x$  saturation from wildfire emissions in some locations of the west. Although outside the scope of this work, we also found that the NACC/GFSv16-CMAQ system yields reasonable results when comparing fire-enhanced  $\text{O}_3$  and  $\text{PM}_{2.5}$  concentrations to aircraft measurements during the 2019 Fire Influence on Regional to Global Environments and Air Quality (FIREX-AQ) field campaign (<https://csl.noaa.gov/projects/firex-aq/>, last access: 5 April 2022) (not shown). The widespread decreases in both the hourly and MDA8  $\text{O}_3$  over all oceanic regions in the domain are driven by the updated halogen (e.g., bromine and iodine chemistry) mediated  $\text{O}_3$  loss in NACC-CMAQ, which can reduce annual mean surface ozone over seawater by 25 % (Sarwar et al., 2019).

There are both relatively large increases (north, northeast, and west) and decreases (south, southeast, and parts of the

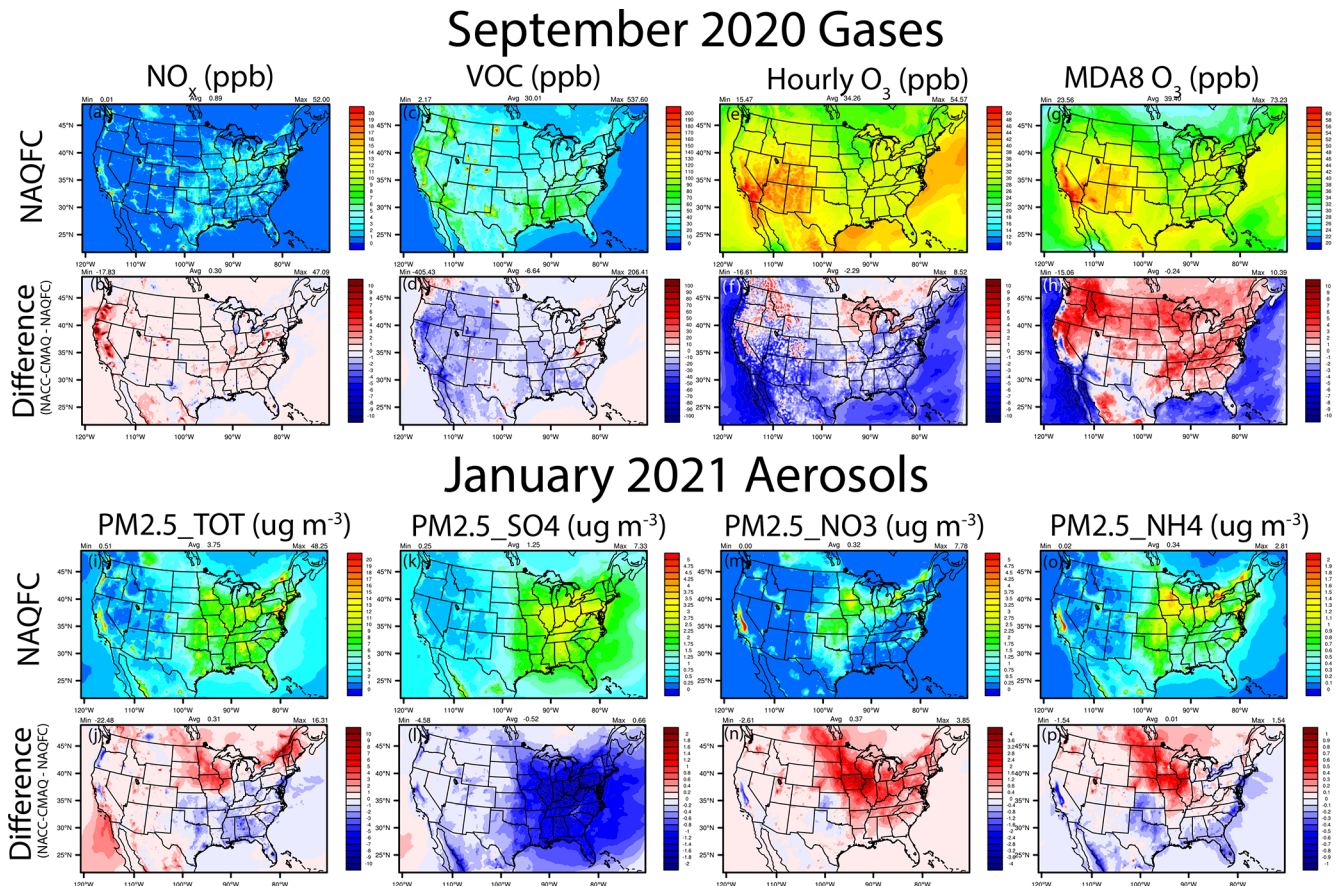


**Figure 13.** Average September 2020  $\text{NO}_x$ , total VOCs, hourly  $\text{O}_3$ , and MDA8  $\text{O}_3$  and January 2021  $\text{PM}_{2.5\_TOT}$ ,  $\text{PM}_{2.5\_SO4}$ ,  $\text{PM}_{2.5\_NO3}$ , and  $\text{PM}_{2.5\_NH4}$  for the prior NAQFC and the absolute differences for NACC-CMAQ–NAQFC.

west) for winter (January 2021) total  $\text{PM}_{2.5}$  ( $\text{PM}_{2.5\_TOT}$ ) in the CONUS for NACC-CMAQ compared to NAQFC (Fig. 13i–j). The decreases in inorganic  $\text{PM}_{2.5\_TOT}$  in the east and southeast are dominated by decreases in particulate sulfate ( $\text{PM}_{2.5\_SO4}$ ) and ammonium ( $\text{PM}_{2.5\_NH4}$ ), while the increases in the northern central and eastern CONUS are driven by increases in particulate nitrate ( $\text{PM}_{2.5\_NO3}$ ) and  $\text{PM}_{2.5\_NH4}$ . Further analysis indicates that the widespread decreases in  $\text{PM}_{2.5\_SO4}$  (strongest in the east) are driven strongly by widespread lower CFRAC in GFSv16 (Fig. 4o–p) and lower aqueous-phase oxidation in CMAQ (not shown). There are also contributions from decreased  $\text{SO}_2$  emissions found in some CONUS regions for NACC-CMAQ (e.g., the northeast; Fig. 11c). Additional consumption of inorganic sulfate as secondary isoprene epoxydiol (IEPOX) organosulfates are formed in the updated AERO7 aerosol mechanism in NACC-CMAQ (Table 1; Pye et al., 2013, 2017), and these further contribute to the  $\text{PM}_{2.5\_SO4}$  decreases. The higher total PRECIP for NACC-CMAQ (Fig. 5) also leads to lower  $\text{PM}_{2.5\_TOT}$  in the eastern and southeastern regions.

The largest  $\text{PM}_{2.5\_TOT}$  increases in the northern central CONUS are primarily driven by enhanced ammonium nitrate formation,  $\text{PM}_{2.5\_NO3}$ , and  $\text{PM}_{2.5\_NH4}$ , which are influenced by increases in  $\text{NH}_3$  emissions (Fig. 11) and the inclusion of BIDI- $\text{NH}_3$  fluxes in NACC-CMAQ (Table 1). BIDI- $\text{NH}_3$  in NACC-CMAQ allows for inline calculation of the diurnal pattern of both  $\text{NH}_3$  evasion (emission) and deposition, while the prior NAQFC only includes deposition. Consequently, BIDI- $\text{NH}_3$  in NACC-CMAQ generally increases ambient  $\text{NH}_4^+$  and  $\text{NO}_3^-$  aerosol concentrations (Bash et al., 2013; Pleim et al., 2019) compared to the prior NAQFC.

There are also contributions to the increased  $\text{PM}_{2.5\_TOT}$  from organic carbon sources (Fig. S25;  $\text{PM}_{2.5\_OC}$ ), especially in the northeastern portion of the domain that include the St. Lawrence River valley region. This is in part due to enhanced anthropogenic VOC emissions in NEIC2016v1 (Fig. 11e, e.g., formaldehyde; not shown) and enhanced AERO7 secondary organic aerosol formation in this region for NACC-CMAQ (not shown). There are also small  $\text{PM}_{2.5\_EC}$  contributions to the  $\text{PM}_{2.5\_TOT}$  decreases in the east and increases in the west for NACC-CMAQ (Fig. S25), which are mainly due to decreases in anthropogenic PEC

**Table 3.** Average September 2020 hourly O<sub>3</sub> evaluation of the operational NAQFC and NACC-CMAQ day 1 forecasts against the AirNow network in different CONUS regions (based on <https://www.epa.gov/aboutepa/regional-and-geographic-offices>, last access: 5 April 2022). Statistical benchmark values based on Emery et al. (2017) are also shown for comparison. Following Emery et al. (2017), a > 40 ppb (i.e., daytime) cutoff for hourly O<sub>3</sub> is applied for the mean observations, mean models, mean bias, and the calculated values of NMB and NME but not for the correlation value (*r*) or index of agreement (IOA). The total number of observation–model pairs is based on all values (i.e., no cutoff). Bold font indicates statistical values outside of the Emery et al. (2017) criteria. Italic font indicates improved NACC-CMAQ performance. Tables S5–S10 provide day 2 and day 3 (NACC-CMAQ only) forecast evaluations.

Day 1 Forecasts	Total no. of pairs	Mean obs (ppb)	Mean mod (ppb)	Mean bias (ppb)	NMB (%)	NME (%)	Corr ( <i>r</i> )	IOA
Benchmark: Emery et al. (2017)	–	–	–	–	Goal: < ±5 %; criteria: < ±15 %	Goal: < 15 %; criteria: < 25 %	Goal: > 0.75; criteria: > 0.50	–
Region 1 (northeast)								
NAQFC	35 983	46.85	43.55	−3.31	−7.06	15.04	0.61	0.71
NACC-CMAQ			43.44	−3.42	−7.29	15.14	<i>0.70</i>	<i>0.81</i>
Region 2 (NY–NJ)								
NAQFC	22 944	46.68	42.90	−3.77	−8.09	17.88	0.59	0.72
NACC-CMAQ			45.18	−1.50	−3.21	<i>14.27</i>	<i>0.72</i>	<i>0.81</i>
Region 3 (mid-Atlantic)								
NAQFC	89 069	46.66	44.29	−2.37	−5.09	12.84	0.65	0.73
NACC-CMAQ			45.81	−0.85	−1.83	13.48	<i>0.74</i>	<i>0.82</i>
Region 4 (southeast)								
NAQFC	105 858	44.62	45.93	1.31	2.93	13.37	0.61	0.65
NACC-CMAQ			47.99	3.37	7.55	14.91	<i>0.74</i>	<i>0.75</i>
Region 5 (upper Midwest)								
NAQFC	109 744	46.61	43.84	−2.77	−5.94	13.28	0.69	0.77
NACC-CMAQ			46.59	−0.03	−0.05	<i>10.69</i>	<i>0.77</i>	<i>0.83</i>
Region 6 (south)								
NAQFC	84 005	48.17	47.18	−0.99	−2.06	13.17	0.68	0.75
NACC-CMAQ			47.81	−0.36	−0.75	<i>12.80</i>	<i>0.75</i>	<i>0.81</i>
Region 7 (central Great Plains)								
NAQFC	27 139	44.98	44.84	−0.14	−0.31	10.45	0.76	0.81
NACC-CMAQ			47.18	2.20	4.90	<i>9.54</i>	<i>0.82</i>	<i>0.86</i>
Region 8 (northern Great Plains)								
NAQFC	51 759	48.97	44.64	−4.32	−8.83	13.89	0.71	0.82
NACC-CMAQ			45.08	−3.89	−7.95	14.00	<i>0.72</i>	<i>0.85</i>
Region 9 (west)								
NAQFC	124 051	55.44	50.29	−5.15	−9.29	18.37	0.69	0.79
NACC-CMAQ			46.37	−9.07	<b>−16.37</b>	21.78	<i>0.71</i>	<i>0.83</i>
Region 10 (northwest)								
NAQFC	14 139	48.41	39.37	−9.03	<b>−18.66</b>	21.59	0.61	0.72
NACC-CMAQ			41.70	−6.71	−13.86	<i>19.91</i>	<i>0.66</i>	<i>0.81</i>



## Day 1 Mean Bias (Model-AirNow) Plots and Domain-Wide Statistics

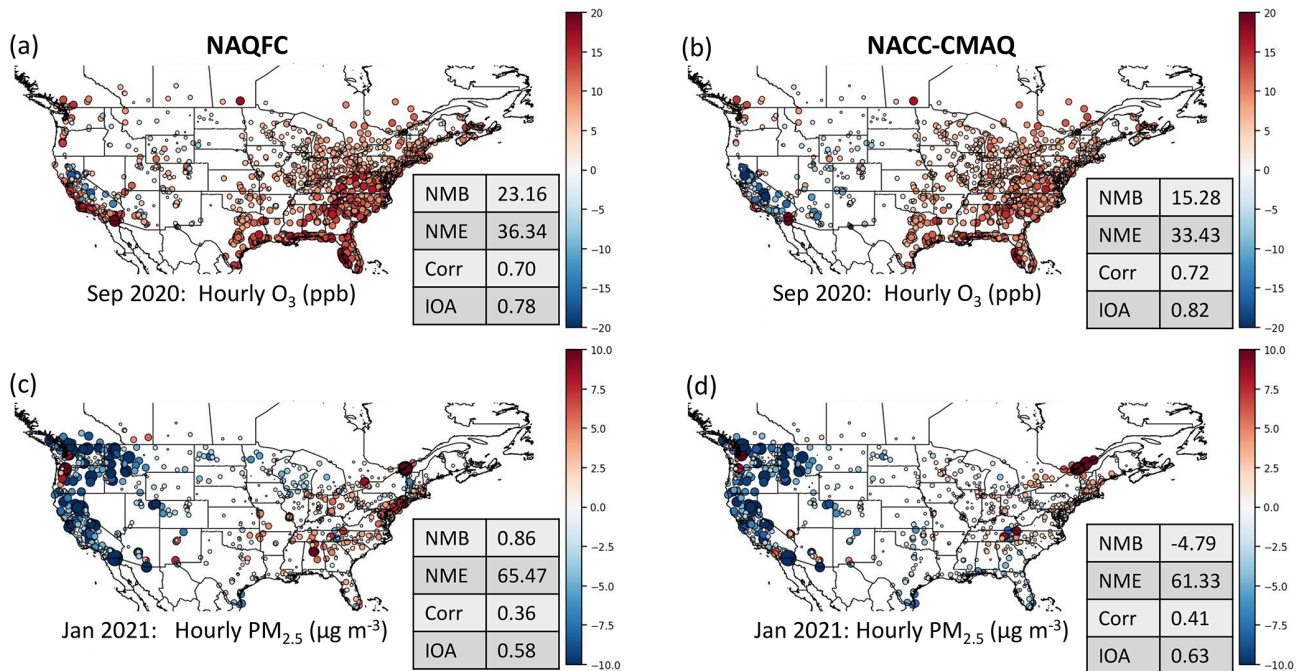


**Figure 14.** Day 1 forecast mean bias plots (model-AirNow) for the current operational NAQFC (a, c) and NACC-CMAQ (b, d) hourly  $O_3$  (a, b) and  $PM_{2.5}$  (c, d) in (a)–(b) September 2020 and (c)–(d) January 2021. Average domain-wide statistics are shown in the tables on the bottom right of each panel.

emissions in the east (Fig. 11g) but also stem from contributions of relatively small GBBEPx PM emissions in the west (not shown). The prior NAQFC does not include biomass burning smoke emissions during the month of January.

#### 4.5 Air quality evaluations and metrics

Evaluation of NACC-CMAQ shows overall improvement in the spatial MB of hourly  $O_3$  (September) and  $PM_{2.5}$  (January) against the AirNow network across CONUS (Fig. 14). There are clear reductions in the NAQFC overpredictions of  $O_3$  and  $PM_{2.5}$  in the east, and overall reduction in NME, and overall improved correlation ( $R$ ) and IOA for NACC-CMAQ. There are also reduced overpredictions in the west for  $O_3$  in September. The shifts to lower concentrations result in larger domain-wide average  $PM_{2.5}$  underpredictions for NACC-CMAQ compared to the prior NAQFC (cf. Fig. 13 above); however, the improvements in  $R$  and IOA for NACC-CMAQ are substantial. The MDA8  $O_3$  spatial MB evaluation against AirNow behaves similarly to NAQFC, with slight degradation in the model performance statistics because of areas of higher overpredictions in the eastern US due to reasons discussed above for enhanced daytime  $O_3$  formation in NACC-CMAQ (Fig. S26).

The day 2 forecasts have similar spatial model performance and statistics, with improved hourly  $O_3$  and  $PM_{2.5}$  model performance (Fig. S27) and slightly higher MDA8

$O_3$  overpredictions in the east for NACC-CMAQ (Fig. S28). The consistent model performance for day 3 also shows utility in extending to 72 h air quality forecasts in the advanced NACC-CMAQ system (Figs. S29–S30). There is, however, a more notable degradation in skill for the day 3 forecast of  $PM_{2.5}$  compared to  $O_3$  in NACC-CMAQ (compare Figs. 14 and S29).

There is significant improvement in the average  $O_3$  and  $PM_{2.5}$  diurnal patterns for each CONUS region other than higher daytime  $O_3$  peaks for NACC-CMAQ compared to prior NAQFC (Fig. 15a–i). This is reflected in the improved  $R$  and IOA over the CONUS on average for NACC-CMAQ (Fig. 14a–b). There is improved day-to-night  $O_3$  transition, i.e., a sharper slope or cutoff of daytime  $O_3$  formation, which leads to lower nighttime  $O_3$  mixing ratios in NACC-CMAQ that agree better with AirNow observations for all CONUS regions.

The NACC-CMAQ  $PM_{2.5}$  diurnal pattern is also more consistent with AirNow for most CONUS regions (Fig. 15k–t), which is supported by improved  $R$  and IOA (Fig. 14c–d). There are, however, some regions (e.g., the northeast, south, and northwest) that the prior NAQFC shows better diurnal performance in this case.

Overall performance evaluations of hourly  $O_3$  in each CONUS region show predominantly improved statistics for NACC-CMAQ, with increased  $R$  and IOA for all regions (Table 3). Comparisons of the NMB, NME, and  $R$  against statis-

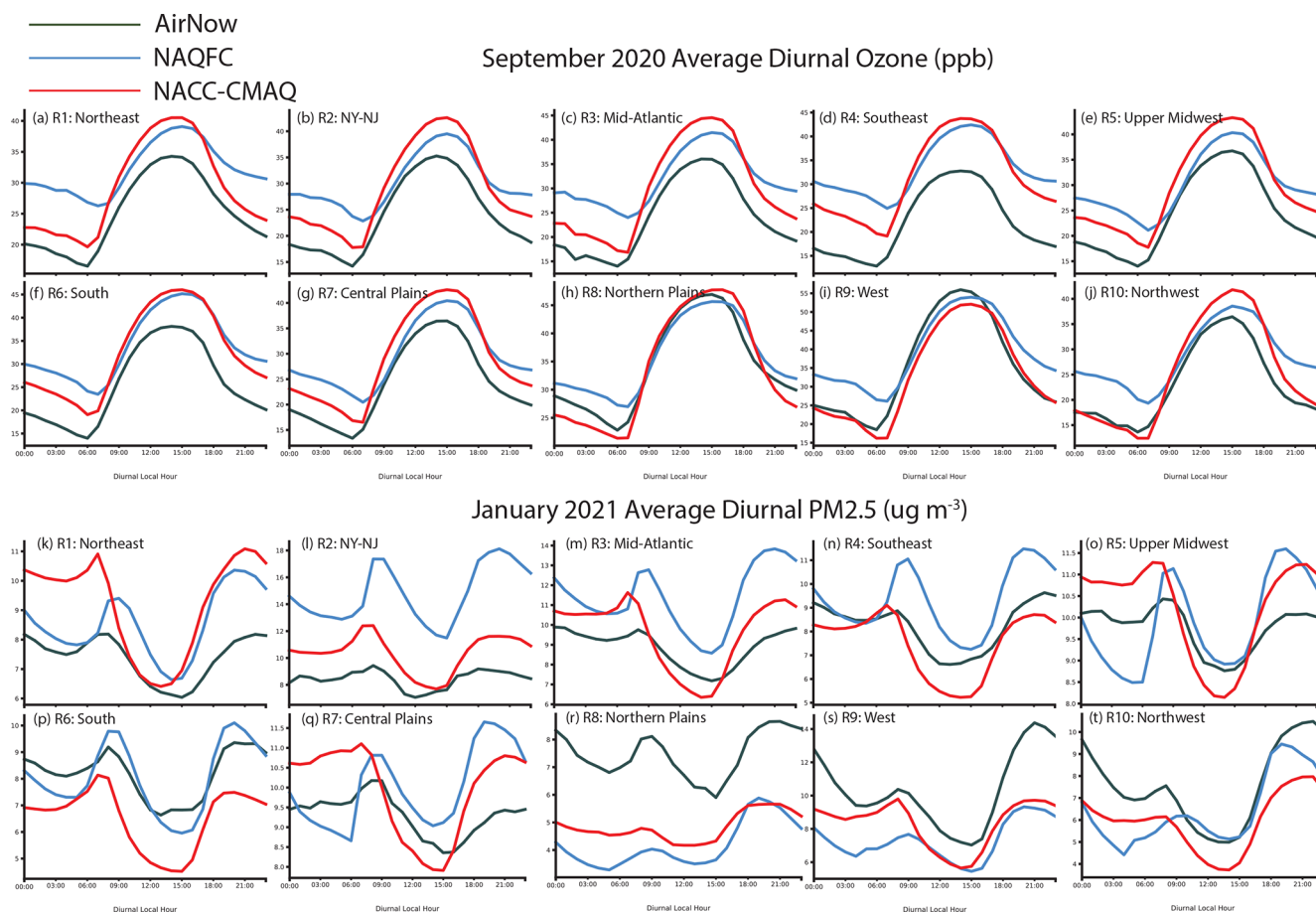


**Figure 15.** Average September 2020 O<sub>3</sub> (top) and January 2021 PM<sub>2.5</sub> (bottom) diurnal patterns for NAQFC (blue), NACC-CMAQ (red), and AirNow observations (green) for different regions in the CONUS. The regions are based on <https://www.epa.gov/aboutepa/regional-and-geographic-offices> (last access: 5 April 2022).

tical benchmark values for photochemical models based on Emery et al. (2017) indicate that both the prior NAQFC and NACC-CMAQ are within specified criteria for hourly O<sub>3</sub> in most regions, except for relatively large NMB values in the west and northwest regions. The increased hourly O<sub>3</sub> underpredictions in NACC-CMAQ degrades the NMB to fail to meet the benchmark in the west but improves the NMB to fall within criteria in the northwest region.

The higher MDA8 O<sub>3</sub> in NACC-CMAQ degrades its regional NMB, NME, and *R* performance slightly compared to the prior NAQFC (Table 4), but *R* and IOA illustrate improvements for most regions, in some cases substantially for *R* (e.g., northeast, southeast, the upper Midwest, and the central Great Plains). The higher daytime O<sub>3</sub> overpredictions by NACC-CMAQ in much of CONUS result in higher NMB and NME values that fall outside of the Emery et al. (2017) benchmark criteria. These remain a concern for both the prior NAQFC and NACC-CMAQ, and efforts are underway to address the persistent daytime O<sub>3</sub> overprediction in the summer, particularly in the eastern US (see Fig. 14a–b and further discussion in Sect. 5).

There are substantial improvements in the overall statistical PM<sub>2.5</sub> performance for NACC-CMAQ, especially for *R* and IOA in most CONUS regions. In many regions where the prior NAQFC falls outside of photochemical criteria values (Emery et al., 2017), NACC-CMAQ shows significant improvement to fall within the criteria. This demonstrates a substantial improvement in the accuracy of the NACC-CMAQ system for PM<sub>2.5</sub> predictions (outside of major wildfires), attributed to the scientific advancements described above.

The day 2 forecast comparisons of the prior NAQFC and NACC-CMAQ regional statistics are similar to day 1, and the day 3 forecast extension for NACC-CMAQ has utility as its O<sub>3</sub> and PM<sub>2.5</sub> statistics predominantly fall within the benchmark criteria in most regions (Tables S5–S10).

## 5 Conclusions and path forward

An advanced National Air Quality Forecasting Capability (NAQFC) was developed and evaluated using NOAA's FV3-based Global Forecast System version 16 (GFSv16) as the

**Table 4.** The same as in Table 3 but for MDA8 O<sub>3</sub>. Note that, as discussed in Emery et al. (2017), cutoff values are not applied for MDA8 O<sub>3</sub>.

Day 1 forecasts	Total no. of pairs	Mean obs (ppb)	Mean mod (ppb)	Mean bias (ppb)	NMB (%)	NME (%)	Corr ( <i>r</i> )	IOA
Benchmark: Emery et al. (2017)	–	–	–	–	Goal: < ±5 %; criteria: < ±15 %	Goal: < 15 %; criteria: < 25 %	Goal: > 0.75; criteria: > 0.50	–
Region 1 (northeast)								
NAQFC	1680	33.05	38.45	5.40	16.35	22.60	0.66	0.73
NACC-CMAQ			38.60	5.55	16.81	21.57	0.73	0.75
Region 2 (NY–NJ)								
NAQFC	1158	32.79	37.07	4.29	13.08	21.38	0.66	0.76
NACC-CMAQ			39.22	6.44	19.63	23.65	0.74	0.75
Region 3 (mid-Atlantic)								
NAQFC	4243	33.85	39.35	5.50	16.24	20.75	0.74	0.77
NACC-CMAQ			41.31	7.46	22.05	24.54	0.76	0.75
Region 4 (southeast)								
NAQFC	5076	31.01	40.30	9.29	29.95	31.83	0.64	0.64
NACC-CMAQ			41.06	10.05	32.41	33.40	0.74	0.67
Region 5 (upper Midwest)								
NAQFC	5210	34.08	37.88	3.80	11.16	18.51	0.75	0.82
NACC-CMAQ			39.89	5.81	17.06	19.94	0.82	0.82
Region 6 (south)								
NAQFC	3901	35.65	42.37	6.72	18.84	23.91	0.74	0.77
NACC-CMAQ			43.01	7.35	20.63	24.35	0.78	0.78
Region 7 (central Great Plains)								
NAQFC	1256	33.37	37.83	4.46	13.36	17.99	0.78	0.82
NACC-CMAQ			39.36	6.00	17.97	19.86	0.85	0.84
Region 8 (northern Great Plains)								
NAQFC	2379	44.18	43.51	−0.47	−1.07	12.84	0.74	0.85
NACC-CMAQ			44.95	0.78	1.76	11.78	0.79	0.88
Region 9 (west)								
5757	51.03	51.26	0.23	0.44	17.84	0.70	0.82	
NACC-CMAQ			48.03	−3.00	−5.88	18.73	0.68	0.79
Region 10 (northwest)								
NAQFC	698	33.13	35.46	2.33	7.03	25.11	0.63	0.72
NACC-CMAQ			36.66	3.53	10.67	25.58	0.59	0.74

driving meteorology for a state-of-the-science Community Multiscale Air Quality (CMAQ) model version 5.3.1. A key component of this new system is the development of the NOAA-EPA Atmosphere Chemistry Coupler (NACC), which forms the bridge between the GFSv16 meteorolog-

ical fields and the CMAQ inputs for improved chemical predictions (i.e., NACC-CMAQ). Such advancements of the NACC-CMAQ system include high-resolution satellite vegetation inputs, with a rapid-refresh VIIRS greenness vegetation fraction and VIIRS climatological leaf area index,

**Table 5.** The same as in Table 3 but for 24 h average PM<sub>2.5</sub>. Note that, as discussed in Emery et al. (2017), cutoff values are not applied for 24 h average PM<sub>2.5</sub>.

Day 1 forecasts	Total no. of pairs	Mean obs (ppb)	Mean mod (ppb)	Mean bias (ppb)	NMB (%)	NME (%)	Corr ( <i>r</i> )	IOA
Benchmark: Emery et al. (2017)	–	–	–	–	Goal: < ±10%; criteria: < ±30%	Goal: < 35%; criteria: < 50%	Goal: > 0.70; criteria: > 0.40	–
Region 1 (northeast)								
NAQFC	1261	7.43	8.47	1.04	13.98	42.57	0.77	0.85
NACC-CMAQ			9.39	1.95	26.30	46.17	0.75	0.83
Region 2 (NY–NJ)								
NAQFC	598	8.54	15.39	6.85	80.25	89.21	0.72	0.55
NACC-CMAQ			10.84	2.30	26.90	47.60	0.77	0.74
Region 3 (mid-Atlantic)								
NAQFC	1897	9.16	11.95	2.79	30.43	42.57	0.81	0.84
NACC-CMAQ			10.16	1.00	10.96	33.24	0.83	0.89
Region 4 (southeast)								
NAQFC	3621	8.45	9.67	1.23	14.53	40.44	0.41	0.62
NACC-CMAQ			7.86	−0.59	−6.98	37.19	0.48	0.67
Region 5 (upper Midwest)								
NAQFC	3270	9.61	9.79	0.19	1.93	38.09	0.58	0.75
NACC-CMAQ			9.65	0.04	0.46	31.42	0.72	0.84
Region 6 (south)								
NAQFC	2101	8.39	7.95	−0.44	−5.19	46.68	0.28	0.57
NACC-CMAQ			6.39	−2.00	−23.82	43.30	0.36	0.59
Region 7 (central Great Plains)								
NAQFC	926	8.67	9.83	1.16	13.41	49.67	0.32	0.58
NACC-CMAQ			8.79	0.12	1.40	32.13	0.68	0.82
Region 8 (northern Great Plains)								
NAQFC	1790	7.66	4.36	−3.30	−43.13	60.51	0.33	0.55
NACC-CMAQ			4.89	−2.77	−36.20	52.68	0.49	0.67
Region 9 (west)								
NAQFC	4118	10.09	7.04	−3.05	−30.27	46.97	0.61	0.74
NACC-CMAQ			7.98	−2.11	−20.89	50.69	0.56	0.73
Region 10 (northwest)								
NAQFC	3922	7.93	6.86	−1.07	−13.54	78.99	0.20	0.46
NACC-CMAQ			6.33	−1.60	−20.19	71.73	0.23	0.49

as well as additional soil data inputs to an improved wind-blown dust (FENGSHA) algorithm in CMAQ. The anthropogenic, biogenic, and wildfire emissions in NACC-CMAQ are also updated compared to the prior NAQFC, and for the first time the forecasting model calculates inline bidirec-

tional NH<sub>3</sub> fluxes. NACC-CMAQ also ingests novel smoke and dust aerosols at its lateral boundaries dynamically from the NOAA operational GEFS-Aerosols model. Finally, the NACC-CMAQ system extends the air quality forecast from 48 to 72 h and provides scientific advances in atmospheric



chemistry modeling to state and local forecasters out to 3 d. The additional day of forecast guidance could aid decision makers to prepare citizens for localized air quality conditions that could adversely affect public health.

Results of the NACC-CMAQ system during recent late summer (September 2020) and winter (January 2021) months show significant changes in both meteorological and chemical predictions compared to the prior NAQFC. The GFSv16 for NACC-CMAQ has a persistently large dry bias (lower Q2) and larger RMSE across much of CONUS in late summer compared to NMMB (i.e., prior NAQFC), which likely stems from excessively dry soil conditions in GFS. GFS is generally cooler in the east and warmer in the west for surface temperature (TEMP2) compared to NMMB, but the overall MB and RMSE are more similar between the models compared to that for Q2. The GFS has a relatively similar planetary boundary layer height (PBLH) at night, but the PBLH in GFSv16 (NACC-CMAQ) is consistently deeper during the daytime peak hours compared to the prior NAQFC.

The differences in surface characteristics, meteorology, and both anthropogenic and natural emissions are driving factors for distinct atmospheric composition differences, where NACC-CMAQ generally outperforms the prior NAQFC for both hourly O<sub>3</sub> and PM<sub>2.5</sub>, especially with improved correlation (*R*) and IOA. This agrees well with significant improvements in the diurnal O<sub>3</sub> and PM<sub>2.5</sub> patterns for NACC-CMAQ, with distinct improvements in the day-to-night O<sub>3</sub> slope and cutoff. While similar overall, the maximum daily 8 h average (MDA8) O<sub>3</sub> is predominantly higher for NACC-CMAQ compared to prior NAQFC, which leads to some forecast degradation due to larger overpredictions of the daytime max O<sub>3</sub>.

The NACC-CMAQ model became the next operational version of the NAQFC at NWS/NOAA on 20 July 2021 and is available on GitHub for continuous integration, future code updates, and potential community research applications. An ongoing comparison and evaluation of the GFSv16/NACC-CMAQ output with a GFSv16-downscaled Weather Research and Forecasting (WRF) version 4 (Skamarock et al., 2019) and CMAQ application will highlight the potential of NACC-CMAQ to serve as an additional community research tool for air quality applications.

While there are substantial advancements in NACC-CMAQ compared to the prior NAQFC, challenges and limitations remain. One need is to bridge the gap from using a VIIRS LAI climatology to a rapid-refresh methodology, i.e., dynamic methodology (similar to the GVF method here), in NACC-CMAQ. There is also a need to consider shifting the paradigm from using “big-leaf” (i.e., homogeneous single layer of phytomass) assumptions that strongly affect the biosphere–atmosphere exchange processes pivotal to both meteorological and chemical model predictions (refer to Bonan et al., 2021). Simple multilayer canopies have been shown to reduce overpredictions of ground-level sur-

face O<sub>3</sub> in the summer due to photolysis attenuation and modified vertical turbulence (Makar et al., 2017), which have significant implications for the daytime O<sub>3</sub> overpredictions in the current and future versions of NAQFC (Figs. 14a–b and S26). We are currently working on similar canopy effects in NACC-CMAQ to reduce the summer O<sub>3</sub> overpredictions in the east and southeast and parts of western CONUS, where there are relatively continuous vegetation structures and canopies (Fig. 14a–b). Other advancements that are important to improving the future versions of the NAQFC include dynamically updated (and weather-dependent) anthropogenic emission sources and improved treatments of mobile sources (e.g., vehicle-induced turbulence; Makar et al., 2021). Further refinements to the inline windblown dust emissions, wildfire smoke emissions, and other process-based natural emissions sources (e.g., lightning NO) are also needed.

Other future directions include migrating the advanced science in the offline 12 km resolution NACC-CMAQ model to a next-generation, high-resolution (e.g., 3 km) inline modeling framework that fits within NOAA’s strategy for the Unified Forecast System (UFS; <https://ufsccommunity.org/>, last access: 5 April 2022). This model system aims to improve integration of atmospheric composition changes with weather predictions, better resolve finer-scale processes, and advance the rapid-refresh techniques for emissions and surface–atmosphere exchange processes. At this time, NACC-CMAQ also does not use dynamic lateral boundary conditions for trace gases and only has dynamically ingested smoke and dust aerosols at its lateral boundaries from the NOAA operational GEFS-Aerosols model. Current work is underway to use next-generation UFS-based global model systems as updated lateral boundary conditions for trace gases in the future of the NAQFC.

Development and implementation of the NACC-CMAQ model is an important step to (i) advance the NAQFC closer to the state of the science for regional air quality forecasting, (ii) improve community applications of NOAA’s FV3GFS-driven atmospheric composition models, and (iii) facilitate the future development of regional high-resolution inline air quality forecasting systems within the UFS framework at NOAA.

*Code and data availability.* The NACC code is publicly available at <https://doi.org/10.5281/zenodo.5507489> (Campbell, 2021a) and via GitHub at <https://github.com/noaa-oar-arl/NACC.git> (last access: 5 April 2022). The modified version of CMAQv5.3.1 used in the advanced NACC-CMAQ model for the next operational NAQFC is available at <https://doi.org/10.5281/zenodo.5507511> (Campbell, 2021b) and via GitHub at <https://github.com/noaa-oar-arl/NAQFC> (last access: 5 April 2022).

The 0.25° FV3-driven Global Forecast System version 16 data (cycled 4× per day) are available in GRIB2 format at <https://www.nco.ncep.noaa.gov/pmb/products/gfs/> (NOAA/NWS, 2022a). The hourly GFSv16 data in gridded NetCDF (~ 13 ×

13 km globally) format and the Gaussian projection that are directly used to drive NACC-CMAQ are also currently being migrated to the Amazon Web Services (AWS) Cloud for improved NOAA community air quality research applications. The advanced NACC-CMAQ data, i.e., the current operational NAQFC version as of 20 July 2021, are available for operational (<https://airquality.weather.gov/>, NOAA/NWS, 2022b) and interactive (<https://digital.mdl.nws.noaa.gov/airquality/#>, NOAA/NWS, 2022c) display from NWS/NOAA. The official NOAA/EMC verification and diagnostics for the NAQFC system are found at [https://www.emc.ncep.noaa.gov/mmb/qa/verification\\_diagnostics/cmaq\\_verf/](https://www.emc.ncep.noaa.gov/mmb/qa/verification_diagnostics/cmaq_verf/) (NOAA/NWS, 2022d).

*Supplement.* The supplement related to this article is available online at: <https://doi.org/10.5194/gmd-15-3281-2022-supplement>.

*Author contributions.* PCC contributed to project conceptualization, methodology, software, data curation, visualization, investigation, and writing of the original draft. YT contributed to project methodology, software, data curation, and investigation. PL contributed to project supervision, project administration, and funding acquisition. BB contributed to project methodology, software, and data curation. DT contributed to project methodology, software, reviewing and editing the paper, project administration, and funding acquisition. RS contributed to project supervision, project administration, funding acquisition, and reviewing and editing the paper. AS contributed to project supervision, project administration, and funding acquisition. JH contributed to project software, and data curation. H-CH contributed to project methodology, software, and data curation. JM contributed to project administration and funding acquisition. LP contributed to project software and data curation. ES contributed to project software, data curation, and reviewing and editing the paper. IS contributed to project administration and funding acquisition. JS contributed to project administration. JT-D contributed to project administration. YJ contributed to project administration and funding acquisition. FY contributed to project administration. TS contributed to project methodology, software, and reviewing and editing the paper. RG contributed to project software and data curation.

*Competing interests.* The contact author has declared that neither they nor their co-authors have any competing interests.

*Disclaimer.* The scientific results and conclusions, as well as any views or opinions expressed herein, are those of the author(s) and do not necessarily reflect the views of NOAA or the Department of Commerce. The research presented was not funded by the EPA and was not subject to the EPA's quality system requirements. The views expressed in this article are those of the author(s) and do not necessarily represent the views or the policies of the US Environmental Protection Agency.

Publisher's note: Copernicus Publications remains neutral with regard to jurisdictional claims in published maps and institutional affiliations.

*Financial support.* This study was co-funded by the National Oceanic and Atmospheric Administration, the University of Maryland, and George Mason University under the Cooperative Institute for Satellite Earth System Studies (CISSSS).

*Review statement.* This paper was edited by Patrick Jöckel and reviewed by two anonymous referees.

## References

- Alexander, B., Park, R. J., Jacob, D. J., and Gong, S.: Transition metal-catalyzed oxidation of atmospheric sulfur: global implications for the sulfur budget, *J. Geophys. Res.*, 114, D02309, <https://doi.org/10.1029/2008JD010486>, 2009.
- American Lung Association: Urban air pollution and health inequities: a workshop report, *Environ Health Perspect.*, 109 Suppl 3, 357–374, PMID: 11427385, PMCID: PMC1240553, <https://doi.org/10.2307/3434783>, 2001.
- Appel, K. W., Gilliam, R. C., Davis, N., Zubrow, A., and Howard, S. C.: Overview of the atmospheric model evaluation tool (amet) v1.1 for evaluating meteorological and air quality models, *Environ. Model. Softw.*, 26, 434–443, <https://doi.org/10.1016/j.envsoft.2010.09.007>, 2011.
- Appel, K. W., Bash, J. O., Fahey, K. M., Foley, K. M., Gilliam, R. C., Hogrefe, C., Hutzell, W. T., Kang, D., Mathur, R., Murphy, B. N., Napelenok, S. L., Nolte, C. G., Pleim, J. E., Pouliot, G. A., Pye, H. O. T., Ran, L., Roselle, S. J., Sarwar, G., Schwede, D. B., Sidi, F. I., Spero, T. L., and Wong, D. C.: The Community Multiscale Air Quality (CMAQ) model versions 5.3 and 5.3.1: system updates and evaluation, *Geosci. Model Dev.*, 14, 2867–2897, <https://doi.org/10.5194/gmd-14-2867-2021>, 2021.
- Astitha, M., Luo, H., Rao, S. T., Hogrefe, C., Mathur, R., and Kumar, N.: Dynamic evaluation of two decades of WRF-CMAQ ozone simulations over the contiguous United States, *Atmos. Environ.*, 164, 102–116, <https://doi.org/10.1016/j.atmosenv.2017.05.020>, 2017.
- Bai, L., Wang, J., Ma, X., and Lu, H.: Air Pollution Forecasts: An Overview, *Int. J. Env. Res. Pub. He.*, 15, 780, <https://doi.org/10.3390/ijerph15040780>, 2018.
- Baker, B. and Pan, L.: Overview of the Model and Observation Evaluation Toolkit (MONET) Version 1.0 for Evaluating Atmospheric Transport Models, *Atmosphere*, 8, 210, <https://doi.org/10.3390/atmos8110210>, 2017.
- Bash, J. O., Walker, J. T., Katul, G. G., Jones, M. R., Nemitz, E., and Robarge, W. P.: Estimation of In-Canopy Ammonia Sources and Sinks in a Fertilized Zea mays Field, *Environ. Sci. Technol.*, 44, 1683–1689, <https://doi.org/10.1021/es9037269>, 2010.
- Bash, J. O., Cooter, E. J., Dennis, R. L., Walker, J. T., and Pleim, J. E.: Evaluation of a regional air-quality model with bidirectional NH<sub>3</sub> exchange coupled to an agroecosystem model, *Biogeosciences*, 10, 1635–1645, <https://doi.org/10.5194/bg-10-1635-2013>, 2013.
- Bash, J. O., Baker, K. R., and Beaver, M. R.: Evaluation of improved land use and canopy representation in BEIS v3.61 with biogenic VOC measurements in California, *Geosci. Model Dev.*, 9, 2191–2207, <https://doi.org/10.5194/gmd-9-2191-2016>, 2016.

- Binkowski, F. S., Arunachalam, S., Adelman, Z., and Pinto, J.: Examining photolysis rates with a prototype on-line photolysis module in CMAQ, *J. Appl. Meteorol. Clim.*, 46, 1252–1256, <https://doi.org/10.1175/JAM2531.1>, 2007.
- Black, T. L.: The new NMC meso-scale Eta Model: description and forecast examples, *Weather Forecast.*, 9, 265–278, [https://doi.org/10.1175/1520-0434\(1994\)009<0265:TNNMEM>2.0.CO;2](https://doi.org/10.1175/1520-0434(1994)009<0265:TNNMEM>2.0.CO;2), 1994.
- Bonan, G. B., Patton, E. G., Finnigan, J. J., Baldocchi, D. D., and Harman, I. N.: Moving beyond the incorrect but useful paradigm: reevaluating big-leaf and multilayer plant canopies to model biosphere-atmosphere fluxes – a review, *Agr. Forest Meteorol.*, 306, 108435, <https://doi.org/10.1016/j.agrformet.2021.108435>, 2021.
- Briggs, G. A.: A plume rise model compared with observations, *J. Air Pollut. Control Assoc.*, 15, 433–438, <https://doi.org/10.1080/00022470.1965.10468404>, 1965.
- Byun, D. and Schere, K. L.: Review of the governing equations, computational algorithms, and other components of the models-3 community multiscale air quality (CMAQ) modeling system, *Appl. Mech. Rev.*, 59, 51–77, <https://doi.org/10.1115/1.2128636>, 2006.
- Byun, D. W. and Ching, J. K. S.: Science algorithms of the EPA Models-3 Community Multi-scale Air Quality (CMAQ) modeling system, EPA/600/R-99/030, Office of Research and Development, US Environmental Protection Agency, [https://cfpub.epa.gov/si/si\\_public\\_record\\_report.cfm?dirEntryId=63400&Lab=NERL](https://cfpub.epa.gov/si/si_public_record_report.cfm?dirEntryId=63400&Lab=NERL) (last access: 5 April 2022), 1999.
- Campbell, G. S. and Norman J. M.: An introduction to environmental biophysics, Springer, 5, ISBN 978-0-387-94937-6, 1998.
- Campbell, P., Zhang, Y., Yahya, K., Wang, K., Hogrefe, C., Pouliot, G., Knote, C., Hodzic, A., San Jose, R., Perez, J., Guerrero, P., Baro, R., and Makar, P.: A Multi-Model Assessment for the 2006 and 2010 Simulations under the Air Quality Model Evaluation International Initiative (AQMEII) Phase 2 over North America: Part I. Indicators of the Sensitivity of O<sub>3</sub> and PM<sub>2.5</sub> Formation Regimes, *Atmos. Environ.*, 115, 569–586, <https://doi.org/10.1016/j.atmosenv.2014.12.026>, 2015.
- Campbell, P. C.: The NOAA-EPA Atmosphere-Chemistry Coupler (NACC), Zenodo [code], <https://doi.org/10.5281/zenodo.5507489>, 2021a.
- Campbell, P. C.: The Advanced National Air Quality Forecast Capability (NAQFC), Zenodo [code], <https://doi.org/10.5281/zenodo.5507511>, 2021b.
- Campbell, P. C., Bash, J. O., and Spero, T. L.: Updates to the Noah land surface model in WRF-CMAQ to improve simulated meteorology, air quality, and deposition, *J. Adv. Model. Earth Sy.*, 11, 231–256, <https://doi.org/10.1029/2018MS001422> 2019.
- Campbell, P. C., Tong, D., Tang, Y., Baker, B., Lee, P., Saylor, R., Stein, A., Ma, S., and Qu, Z.: Impacts of the COVID-19 Economic Slowdown on Ozone Pollution in the U.S., *Atmos. Environ.*, 264, 118713, <https://doi.org/10.1016/j.atmosenv.2021.118713>, 2021.
- Chen, F. and Dudhia, J.: Coupling an advanced land surface-hydrology model with the Penn State-NCAR MM5 modeling system. Part I: Model implementation and sensitivity, *Mon. Weather Rev.*, 129, 569–585, [https://doi.org/10.1175/1520-0493\(2001\)129<0569:CAALSH>2.0.CO;2](https://doi.org/10.1175/1520-0493(2001)129<0569:CAALSH>2.0.CO;2), 2001.
- Chen, J.-H. and Lin, S.-J.: The remarkable predictability of inter-annual variability of Atlantic hurricanes during the past decade, *Geophys. Res. Lett.*, 38, L11804, <https://doi.org/10.1029/2011GL047629>, 2011.
- Chen, J.-H. and Lin, S.-J.: Seasonal predictions of tropical cyclones using a 25 km-resolution general circulation model, *J. Climate*, 26, 380–398, <https://doi.org/10.1175/JCLI-D-12-00061.1>, 2013.
- Chen, J.-H., Lin, S.-J., Zhou, L., Chen, X., Rees, S. L., Bender, M., and Morin, M.: Evaluation of Tropical Cyclone Forecasts in the Next Generation Global Prediction System, *Mon. Weather Rev.*, 147, 3409–3428, <https://doi.org/10.1175/MWR-D-18-0227.1>, 2019.
- Chen, X., Andronova, N., Van Leer, B., Penner, J. E., Boyd, J. P., Jablonowski, C., and Lin, S.: A Control-Volume Model of the Compressible Euler Equations with a Vertical Lagrangian Coordinate, *Mon. Weather Rev.*, 141, 2526–2544, <https://doi.org/10.1175/MWR-D-12-00129.1>, 2013.
- Chen, X., Zhang, Y., Wang, K., Tong, D., Lee, P., Tang, Y., Huang, J., Campbell, P. C., McQueen, J., Pye, H. O. T., Murphy, B. N., and Kang, D.: Evaluation of the offline-coupled GFSv15–FV3–CMAQv5.0.2 in support of the next-generation National Air Quality Forecast Capability over the contiguous United States, *Geosci. Model Dev.*, 14, 3969–3993, <https://doi.org/10.5194/gmd-14-3969-2021>, 2021.
- Chin, M., Rood, R. B., Lin, S.-J., Muller, J. F., and Thomsson, A. M.: Atmospheric sulfur cycle in the global model GOCART: Model description and global properties, *J. Geophys. Res.*, 105, 24671–24687, <https://doi.org/10.1029/2000JD900384>, 2000.
- Chin, M., Ginoux, P., Kinne, S., Holben, B. N., Duncan, B. N., Martin, R. V., Logan, J. A., Akiko, H., and Nakajima, T.: Tropospheric aerosol optical thickness from the GOCART model and comparisons with satellite and sun photometer measurements, *J. Atmos. Sci.*, 59, 461–483, [https://doi.org/10.1175/1520-0469\(2002\)059<0461:TAOTFT>2.0.CO;2](https://doi.org/10.1175/1520-0469(2002)059<0461:TAOTFT>2.0.CO;2), 2002.
- Chinese State Council: Air Pollution Prevention and Control Action Plan (Guo Fa [2013] No. 37, <http://en.cleanairchina.org/file/loadFile/26.html> (last access: 5 April 2022), 2013.
- Clough, S. A., Shephard, M. W., Mlawer, J. E., Delamere, J. S., Iacono, M. J., Cady-Pereira, K., Boukabara, S., and Brown, P. D.: Atmospheric radiative transfer modeling: A summary of the AER codes, *J. Quant. Spectrosc. Ra.*, 91, 233–244, <https://doi.org/10.1016/j.jqsrt.2004.05.058>, 2005.
- Cooter, E. J., Bash, J. O., Walker, J. T., Jones, M. R., and Robarge, W.: Estimation of NH<sub>3</sub> bi-directional flux from managed agricultural soils, *Atmos. Environ.*, 44, 2107–2115, <https://doi.org/10.1016/j.atmosenv.2010.02.044>, 2010.
- Cooter, E. J., Bash, J. O., Benson, V., and Ran, L.: Linking agricultural crop management and air quality models for regional to national-scale nitrogen assessments, *Biogeosciences*, 9, 4023–4035, <https://doi.org/10.5194/bg-9-4023-2012>, 2012.
- Demetriou, C. A. and Vineis, P.: Carcinogenicity of ambient air pollution: use of biomarkers, lessons learnt and future directions, *J. Thorac. Dis.*, 7, 67–95, <https://doi.org/10.3978/j.issn.2072-1439.2014.12.31>, 2015.
- Ding, H. and Zhu, Y.: NDE Vegetation Products System Algorithm Theoretical Basis Document, Version 4.0. NOAA/NESDIS/OSPO, [https://www.ospo.noaa.gov/Products/documents/GVF\\_ATBD\\_V4.0.pdf](https://www.ospo.noaa.gov/Products/documents/GVF_ATBD_V4.0.pdf) (last access: 2 February 2021), 2018.

- Dong, X., Fu, J. S., Huang, K., Tong, D., and Zhuang, G.: Model development of dust emission and heterogeneous chemistry within the Community Multiscale Air Quality modeling system and its application over East Asia, *Atmos. Chem. Phys.*, 16, 8157–8180, <https://doi.org/10.5194/acp-16-8157-2016>, 2016.
- Driemel, A., Augustine, J., Behrens, K., Colle, S., Cox, C., Cuevas-Agulló, E., Denn, F. M., Duprat, T., Fukuda, M., Grobe, H., Haefelin, M., Hodges, G., Hyett, N., Ijima, O., Kallis, A., Knap, W., Kustov, V., Long, C. N., Longenecker, D., Lupi, A., Maturilli, M., Mimouni, M., Ntsangwane, L., Ogihara, H., Olano, X., Olfes, M., Omori, M., Passamani, L., Pereira, E. B., Schmithüsen, H., Schumacher, S., Sieger, R., Tamlyn, J., Vogt, R., Vuilleumier, L., Xia, X., Ohmura, A., and König-Langlo, G.: Baseline Surface Radiation Network (BSRN): structure and data description (1992–2017), *Earth Syst. Sci. Data*, 10, 1491–1501, <https://doi.org/10.5194/essd-10-1491-2018>, 2018.
- Eder, B., Kang, D., Mathur, R., Yu, S., and Schere, K.: An operational evaluation of the Eta-CMAQ air quality forecast model, *Atmos. Environ.*, 40, 4894–4905, <https://doi.org/10.1016/j.atmosenv.2005.12.062>, 2006.
- Eder, B., Kang, D., Mathur, R., Pleim, J., Yu, S., Otte, T., and Pouliot, G.: A performance evaluation of the National Air Quality Forecast Capability for the summer of 2007, *Atmos. Environ.*, 43, 2312–2320, <https://doi.org/10.1016/j.atmosenv.2009.01.033>, 2009.
- Ek, M., Mitchell, B. K. E., Lin, Y., Rogers, E., Grunmann, P., Koren, V., Gayno, G., and Tarpley, J. D.: Implementation of Noah land surface model advances in the National Centers for Environmental Prediction operational mesoscale Eta model, *J. Geophys. Res.*, 108, 8851, <https://doi.org/10.1029/2002JD003296>, 2003.
- Emery, C., Liu, Z., Russell, A. G., Odman, M. T., Yarwood, G., and Kumar, N.: Recommendations on statistics and benchmarks to assess photochemical model performance, *J. Air Waste Manage. Assoc.*, 67, 582–598, <https://doi.org/10.1080/10962247.2016.1265027>, 2017.
- Finkelstein, M. M., Jerrett, M., DeLuca, P., Finkelstein, N., Verma, D. K., Chapman, K., and Sears, M. R.: Relation between income, air pollution and mortality: A cohort study, *Can. Med. Assoc. J.*, 169, 397–402, 2003.
- Fu, X., Wang, S. X., Cheng, Z., Xing, J., Zhao, B., Wang, J. D., and Hao, J. M.: Source, transport and impacts of a heavy dust event in the Yangtze River Delta, China, in 2011, *Atmos. Chem. Phys.*, 14, 1239–1254, <https://doi.org/10.5194/acp-14-1239-2014>, 2014.
- Gantt, B., Kelly, J. T., and Bash, J. O.: Updating sea spray aerosol emissions in the Community Multiscale Air Quality (CMAQ) model version 5.0.2, *Geosci. Model Dev.*, 8, 3733–3746, <https://doi.org/10.5194/gmd-8-3733-2015>, 2015.
- Ginoux, P., Chin, M., Tegen, I., Prospero, J., Holben, B., Dubovik, O., and Lin, S.-J.: Sources and global distributions of dust aerosols simulated with the GOCART model, *J. Geophys. Res.*, 106, 20255–20273, <https://doi.org/10.1029/2000JD000053>, 2001.
- Grell, G. A., Dudhia, J., and Stauffer, D. R.: A description of the fifth-generation Penn State/NCAR Mesoscale Model (MM5), NCAR tech. Note NCAR TN-398-1-STR, 117 pp., <https://doi.org/10.5065/D60Z716B>, 1994.
- Han, J. and Pan, H.-L.: Revision of Convection and Vertical Diffusion Schemes in the NCEP Global Forecast System, *Weather Forecast.*, 26, 520–533, <https://doi.org/10.1175/WAF-D-10-05038.1>, 2011.
- Han, J. and Bretherton, C. S.: TKE-Based Moist Eddy-Diffusivity Mass-Flux (EDMF) Parameterization for Vertical Turbulent Mixing, *Weather Forecast.*, 34, 869–886, <https://doi.org/10.1175/WAF-D-17-0046.1>, 2019.
- Han, J., Wang, W., Kwon, Y. C., Hong, S.-Y., Tallapragada, V., and Yang, F.: Updates in the NCEP GFS Cumulus Convection Schemes with Scale and Aerosol Awareness, *Weather Forecast.*, 32, 2005–2017, <https://doi.org/10.1175/WAF-D-17-0046.1>, 2017.
- Harris, L. M. and Lin, S.: A Two-Way Nested Global-Regional Dynamical Core on the Cubed-Sphere Grid, *Mon. Weather Rev.*, 141, 283–306, <https://doi.org/10.1175/MWR-D-11-00201.1>, 2013.
- Harris, L. M., Lin, S., and Tu, C.: High-Resolution Climate Simulations Using GFDL HiRAM with a Stretched Global Grid, *J. Climate*, 29, 4293–4314, <https://doi.org/10.1175/JCLI-D-15-0389.1>, 2016.
- Huang, J., McQueen, J., Wilczak, J., Djalalova, I., Stajner, I., 60 Shafran, P., Allured, D., Lee, P., Pan, L., Tong, D., Huang, H.-C., DiMego, G., Upadhyay, S., and Monache, L. D.: Improving NOAA NAQFC PM<sub>2.5</sub> Predictions with a Bias Correction Approach, *Weather Forecast.*, 32, 407–421, <https://doi.org/10.1175/WAF-D-16-0118.1>, 2017.
- Huang, J. and McQueen, J.: Development and evaluation of offline coupling of FV3-based GFS with CMAQ at NOAA, The 17th CMAS Conference, 22–24 October 2018, UNC-Chapel Hill, NC, 2018.
- Huang, J., McQueen, J., Yang, B., Shafran, P., Huang, H.-C., Bhat-tacharjee, P., Tang, Y., Campbell, P. C., Tong, D., Lee, P., Stajner, I., Kain, J. S., Tirado-Delgado, J., and Koch, D. M.: A comparison of global scale FV3 versus regional scale NAM meteorological drivers for regional air quality forecastin, The 100th AGU Fall Meeting, 9–13 December 2019, San Francisco, CA, 2019.
- Huang, M., Tong, D., Lee, P., Pan, L., Tang, Y., Stajner, I., Pierce, R. B., McQueen, J., and Wang, J.: Toward enhanced capability for detecting and predicting dust events in the western United States: the Arizona case study, *Atmos. Chem. Phys.*, 15, 12595–12610, <https://doi.org/10.5194/acp-15-12595-2015>, 2015.
- Iacono, M. J., Delamere, J. S., Mlawer, E. J., Shephard, M. W., Clough, S. A., and Collins, W. B.: Radiative forcing by long-lived greenhouse gases: Calculations with the AER radiative transfer models, *J. Geophys. Res.*, 113, D13103, <https://doi.org/10.1029/2008JD009944>, 2008.
- Institute of Medicine: Toward Environmental Justice: Research, Education, and Health Policy Needs, Washington, DC, National Academy Press, <https://doi.org/10.17226/6034>, 1999.
- Janjic, Z. and Gall, R. L.: Scientific documentation of the NCEP nonhydrostatic multiscale model on the B grid (NMMB), Part 1 Dynamics (No. NCAR/TN-489+STR), University Corporation for Atmospheric Research, <https://doi.org/10.5065/D6WH2MZX>, 2012.
- Jimenez, P. A., Dudhia, J., Gonzalez-Rouco, J. F., Navarro, J., Montavez, J. P., and Garcia-Bustamante, E.: A revised scheme for the WRF surface layer formulation, *Mon. Weather Rev.*, 140, 898–918, <https://doi.org/10.1175/MWR-D-11-00056.1>, 2012.
- Kang, D., Eder, B. K., Stein, A. F., Grell, G. A., Peckham, S. E., and McHenry, J.: The New England Air Quality Forecasting Pi-

- lot Program: Development of an Evaluation Protocol and Performance Benchmark, *J. Air Waste Manage. Assoc.*, 55, 1782–1796, <https://doi.org/10.1080/10473289.2005.10464775>, 2005.
- Karamchandani, P., Long, Y., Pirovano, G., Balzarini, A., and Yarwood, G.: Source-sector contributions to European ozone and fine PM in 2010 using AQMEII modeling data, *Atmos. Chem. Phys.*, 17, 5643–5664, <https://doi.org/10.5194/acp-17-5643-2017>, 2017.
- Kar Kurt, O., Zhang, J., and Pinkerton, K. E.: Pulmonary Health Effects of Air Pollution, *Curr. Opin. Pulm. Med.*, 22, 138–143, <https://doi.org/10.1097/MCP.0000000000000248>, 2016.
- Kelly, J. T., Bhave, P. V., Nolte, C. G., Shankar, U., and Foley, K. M.: Simulating emission and chemical evolution of coarse sea-salt particles in the Community Multiscale Air Quality (CMAQ) model, *Geosci. Model Dev.*, 3, 257–273, <https://doi.org/10.5194/gmd-3-257-2010>, 2010.
- Kim, Y., Sartelet, K., and Seigneur, C.: Formation of secondary aerosols over Europe: comparison of two gas-phase chemical mechanisms, *Atmos. Chem. Phys.*, 11, 583–598, <https://doi.org/10.5194/acp-11-583-2011>, 2011a.
- Kim, Y., Couvidat, F., Sartelet, K., and Seigneur, C.: Comparison of different gas phase mechanisms and aerosol modules for simulating particulate matter formation, *J. Air Waste Manage.*, 61, 1218e1226, <https://doi.org/10.1080/10473289.2011.603999>, 2011b.
- Krueger, S. K., Fu, Q., Liou, K. N., and Chin, H.-N. S.: Improvement of an ice-phase microphysics parameterization for use in numerical simulations of tropical convection, *J. Appl. Meteorol.*, 34, 281–287, <https://doi.org/10.1175/1520-0450-34.1.281>, 1995.
- Landrigan, P. J., Fuller, R., Acosta, N. J., Adeyi, O., Arnold, R., Basu, N., Bibi Balde, A., Bertollini, R., Bose-O'Reilly, S., Boufford, J. L., Breysse, P. N., Chiles, T., Mahidol, C., Coll-Seck, A. M., Cropper, M. L., Fobil, J., Fuster, V., Greenstone, M., Haines, A., Hanrahan, D., Hunter, D., Khare, M., Krupnick, A., Lanphear, B., Lohani, B., Martin, K., Mathiasen, K., McTeer, M. A., Murray, C. J. L., Ndahimananjara, J. D., Perera, F., Potocnik, J., Preker, A. S., Ramesh, J., Rockstrom, J., Salinas, C., Samson, L. D., Sandilya, K., Sly, P. D., Smith, K. R., Steiner, A., Stewart, R. B., Suk, W. A., van Schayck, O. C. P., Yadama, G. N., Yumkella, K., and Zhong, M.: The Lancet Commission on pollution and health, *Lancet*, 391, 462–512, [https://doi.org/10.1016/S0140-6736\(17\)32345-0](https://doi.org/10.1016/S0140-6736(17)32345-0), 2018.
- Lee, B.-J., Kim, B., and Lee, K.: Air Pollution Exposure and Cardiovascular Disease, *Toxicol Res.-UK*, 30, 71–75, <https://doi.org/10.5487/TR.2014.30.2.071>, 2014.
- Lee, P., McQueen, J., Stajner, I., Huang, J., Pan, L., Tong, D., Kim, H., Tang, Y., Kondragunta, S., Ruminski, M., Lu, S., Rogers, E., Saylor, R., Shafran, P., Huang, H.-C., Gorline, J., Upadhayay, S., and Artz, R.: NAQFC Developmental Forecast Guidance for Fine Particulate Matter (PM<sub>2.5</sub>), *Weather Forecast.*, 32, 343–360, <https://doi.org/10.1175/waf-d-15-0163.1>, 2017.
- Lin, S.: A “Vertically Lagrangian” Finite-Volume Dynamical Core for Global Models, *Mon. Weather Rev.*, 132, 2293–2307, [https://doi.org/10.1175/1520-0493\(2004\)132<2293:AVLFDC>2.0.CO;2](https://doi.org/10.1175/1520-0493(2004)132<2293:AVLFDC>2.0.CO;2), 2004.
- Lin, S. and Rood, R. B.: Multidimensional Flux-Form Semi-Lagrangian Transport Schemes, *Mon. Weather Rev.*, 124, 2046–2070, [https://doi.org/10.1175/1520-0493\(1996\)124<2046:MFFSLT>2.0.CO;2](https://doi.org/10.1175/1520-0493(1996)124<2046:MFFSLT>2.0.CO;2), 1996.
- Lin, S., Chao, W. C., Sud, Y. C., and Walker, G. K.: A Class of the van Leer-type Transport Schemes and Its Application to the Moisture Transport in a General Circulation Model, *Mon. Weather Rev.*, 122, 1575–1593, [https://doi.org/10.1175/1520-0493\(1994\)122<1575:ACOTVL>2.0.CO;2](https://doi.org/10.1175/1520-0493(1994)122<1575:ACOTVL>2.0.CO;2), 1994.
- Lin, Y.-L., Farley, R. D., and Orville, H. D.: Bulk parameterization of the snow field in a cloud model, *J. Clim. Appl. Meteorol.*, 22, 1065–1092, [https://doi.org/10.1175/1520-0450\(1983\)022<1065:BPOTSF>2.0.CO;2](https://doi.org/10.1175/1520-0450(1983)022<1065:BPOTSF>2.0.CO;2), 1983.
- Liu, Y. and Wang, T.: Worsening urban ozone pollution in China from 2013 to 2017 – Part 1: The complex and varying roles of meteorology, *Atmos. Chem. Phys.*, 20, 6305–6321, <https://doi.org/10.5194/acp-20-6305-2020>, 2020.
- Lord, S. J., Willoughby, H. E., and Piotrowicz, J. M.: Role of a parameterized ice-phase microphysics in an axisymmetric, nonhydrostatic tropical cyclone model, *J. Atmos. Sci.*, 41, 2836–2848, [https://doi.org/10.1175/1520-0469\(1984\)041<2836:ROAPIP>2.0.CO;2](https://doi.org/10.1175/1520-0469(1984)041<2836:ROAPIP>2.0.CO;2), 1984.
- Makar, P. A., Staebler, R., Akingunola, A., Zhang, J., McLinden, C., Kharol, S. K., Pabla, B., Cheung, P., and Zheng, Q.: The effects of forest canopy shading and turbulence on boundary layer ozone, *Nat Commun.*, 8, 15243, <https://doi.org/10.1038/ncomms15243>, 2017.
- Makar, P. A., Stroud, C., Akingunola, A., Zhang, J., Ren, S., Cheung, P., and Zheng, Q.: Vehicle-induced turbulence and atmospheric pollution, *Atmos. Chem. Phys.*, 21, 12291–12316, <https://doi.org/10.5194/acp-21-12291-2021>, 2021.
- Marlier, M. E., Jina, A. S., Kinney, P. L., and DeFries, R. S.: Extreme Air Pollution in Global Megacities, *Curr Clim Change Rep.*, 2, 15–27, <https://doi.org/10.1007/s40641-016-0032-z>, 2016.
- Martin, R. L. and Good, T. W.: Catalyzed oxidation of sulfur dioxide in solution: the iron-manganese synergism, *Atmos. Environ.*, 25A, 2395–2399, [https://doi.org/10.1016/0960-1686\(91\)90113-L](https://doi.org/10.1016/0960-1686(91)90113-L), 1991.
- Massad, R.-S., Nemitz, E., and Sutton, M. A.: Review and parameterisation of bi-directional ammonia exchange between vegetation and the atmosphere, *Atmos. Chem. Phys.*, 10, 10359–10386, <https://doi.org/10.5194/acp-10-10359-2010>, 2010.
- Mathur, R., Yu, S., Kang, D., and Schere, K. L.: Assessment of the wintertime performance of developmental particulate matter forecasts with the Eta-Community Multiscale Air Quality modeling system, *J. Geophys. Res.*, 113, D02303, <https://doi.org/10.1029/2007JD008580>, 2008.
- Matthias, V., Arndt, J. A., Aulinger, A., Bieser, J., Denier van der Gon, H., Kranenburg, R., Kuenen, J., Neumann, D., Pouliot, G., and Quante, M.: Modeling emissions for three-dimensional atmospheric chemistry transport models, *J. Air Waste Manage.*, 68, 763–800, <https://doi.org/10.1080/10962247.2018.1424057>, 2018.
- McKeen, S., Wilczak, J., Grell, G., Djalova, I., Peckham, S., Hsie, E.-Y., Gong, W., Bouchet, V., Menard, S., Moffet, R., McHenry, J., McQueen, J., Tang, Y., Carmichael, G. R., Pagowski, M., Chan, A., Dye, T., Frost, G., Lee, P., and Mathur, R.: Assessment of an ensemble of seven real-time ozone forecasts over eastern North America during the summer of 2004, *J. Geophys. Res.*, 110, D21307, <https://doi.org/10.1029/2005JD005858>, 2005.
- McKeen, S., Chung, S. H., Wilczak, J., Grell, G., Djalalova, I., Peckham, S., Gong, W., Bouchet, V., Moffet, R., Tang, Y.,

- Carmichael, G. R., Mathur, R., and Yu, S.: Evaluation of several PM<sub>2.5</sub> forecast models using data collected during the ICART-T/NEAQS 2004 field study, *J. Geophys. Res.*, 112, D10S20, <https://doi.org/10.1029/2006JD007608>, 2007.
- McKeen, S., Grell, G., Peckham, S., Wilczak, J., Djalalova, I., Hsie, E., Frost, G., Peischl, J., Schwartz, J., Spackman, R., Holloway, J., de Gouw, J., Warneke, C., Gong, W., Bouchet, V., Gaudreault, S., Racine, J., McHenry, J., McQueen, J., Lee, P., Tang, Y., Carmichael, G. R., and Mathur, R.: An evaluation of real-time air quality forecasts and their urban emissions over eastern Texas during the summer of 2006 Second Texas Air Quality Study field study, *J. Geophys. Res.*, 114, D00F11, <https://doi.org/10.1029/2008JD011697>, 2009.
- Miller, J., Safford, H., Crimmins, M., and Thode, A.: Quantitative evidence for increasing forest fire severity in the Sierra Nevada and Southern Cascade Mountains, California and Nevada, USA, *Ecosystems*, 12, 16–32, <https://doi.org/10.1007/s10021-008-9201-9>, 2009.
- Mlawer, E. J., Taubman, S. J., Brown, P. D., Iacono, M. J., and Clough, S. A.: Radiative transfer for inhomogeneous atmosphere: RTM, a validated correlated-k model for the longwave, *J. Geophys. Res.*, 102, 16663–16682, <https://doi.org/10.1029/97JD00237>, 1997.
- Monin, A. S. and Obukhov, A. M.: Basic laws of turbulent mixing in the surface layer of the atmosphere, *Tr. Akad. Nauk SSSR Geophys. Inst.*, 24, 163–187, 1954 (in Russian).
- Myneni, R. and Knyazikhin, Y.: VIIRS/NPP Leaf Area Index/FPAR 8-Day L4 Global 500m SIN Grid V001, NASA EOSDIS Land Processes DAAC [data set], <https://doi.org/10.5067/VIIRS/VNP15A2H.001>, 2018.
- National Emissions Inventory (NEI): NEI 2014v2 Emissions, U.S. EPA Repository [data set], [https://edap.epa.gov/public/extensions/nei\\_report\\_2014/dashboard.html#sector-db](https://edap.epa.gov/public/extensions/nei_report_2014/dashboard.html#sector-db) (last access: 26 February 2020), 2014.
- National Emissions Inventory Collaborative (NEI): 2016v1 Emissions Modeling Platform [data set], <http://views.cira.colostate.edu/wiki/wiki/10202> (last access: 5 April 2022), 2019.
- Nemitz, E., Sutton, M. A., Schjoerring, J. K., Husted, S., and Wyers, G. P.: Resistance modelling of ammonia exchange over oilseed rape, *Agr. Forest Meteorol.*, 105, 405–425, [https://doi.org/10.1016/S0168-1923\(00\)00206-9](https://doi.org/10.1016/S0168-1923(00)00206-9), 2000.
- Niinemets, Ü., Arneth, A., Kuhn, U., Monson, R. K., Peñuelas, J., and Staudt, M.: The emission factor of volatile isoprenoids: stress, acclimation, and developmental responses, *Biogeosciences*, 7, 2203–2223, <https://doi.org/10.5194/bg-7-2203-2010>, 2010.
- NOAA/NWS: Global Forecast System (GFS) Version 16 [data set], <https://www.nco.ncep.noaa.gov/pmb/products/gfs/>, last access: 5 April 2022a.
- NOAA/NWS: Air Quality Forecast Guidance – Operational [data set], <https://airquality.weather.gov/>, last access: 5 April 2022b.
- NOAA/NWS: Air Quality Forecast Guidance – Experimental [data set], <https://digital.mdl.nws.noaa.gov/airquality/>, last access: 5 April 2022c.
- NOAA/NWS: Operational CMAQ Verification – Experimental [data set], [https://www.emc.ncep.noaa.gov/mmb/qaq/verification\\_diagnostics/cmaq\\_verf/](https://www.emc.ncep.noaa.gov/mmb/qaq/verification_diagnostics/cmaq_verf/) last access: 5 April 2022d.
- O'Neill, M. S., Jerrett, M., Kawachi, I., Levy, J. I., Cohen, A. J., Gouveia, N., Wilkinson, P., Fletcher, T., Cifuentes, L., and Schwartz, J.: Health, wealth, and air pollution: Advancing theory and methods, *Environ. Health Persp.*, 111, 1861–1870, <https://doi.org/10.1289/ehp.6334>, 2003.
- Otte, T. L. and Pleim, J. E.: The Meteorology-Chemistry Interface Processor (MCIP) for the CMAQ modeling system: updates through MCIPv3.4.1, *Geosci. Model Dev.*, 3, 243–256, <https://doi.org/10.5194/gmd-3-243-2010>, 2010.
- Otte, T. L., Pouliot, G., Pleim, J. E., Young, J. O., Schere, K. L., Wong, D. C., Lee, P., Tsidulko, M., McQueen, J., Davidson, P., Mathur, R., Chuang, H.-Y., DiMego, G., and Seaman, N. L.: Linking the Eta Model with the Community Multiscale Air Quality (CMAQ) Modeling System to Build a National Air Quality Forecasting System, *Weather Forecast.*, 20, 367–384, <https://doi.org/10.1175/WAF855.1>, 2005.
- Pinder, R. W., Dennis, R. L., and Bhave, P. V.: Observable indicators of the sensitivity of PM<sub>2.5</sub> nitrate to emission reductions: part I. Derivation of the adjusted gas ratio and applicability at regulatory-relevant time scales, *Atmos. Environ.*, 42, 1275e1286, <https://doi.org/10.1016/j.atmosenv.2007.10.039>, 2008.
- Pleim, J. and Ran, L.: Surface flux modeling for air quality applications, *Atmosphere*, 2, 271–302, <https://doi.org/10.3390/atmos2030271>, 2011.
- Pleim, J. E.: A combined local and nonlocal closure model for the atmospheric boundary layer. Part I: Model description and testing, *J. Appl. Meteor. Climatol.*, 46, 1383–1395, <https://doi.org/10.1175/JAM2539.1>, 2007a.
- Pleim, J. E.: A combined local and nonlocal closure model for the atmospheric boundary layer. Part II: Application and evaluation in a mesoscale meteorological model, *J. Appl. Meteorol. Clim.*, 46, 1396–1409, <https://doi.org/10.1175/JAM2534.1>, 2007b.
- Pleim, J. E., Bash, J. O., Walker, J. T., and Cooter, E. J.: Development and evaluation of an ammonia bidirectional flux parameterization for air quality models, *J. Geophys. Res.-Atmos.*, 118, 3794–3806, <https://doi.org/10.1002/jgrd.50262>, 2013.
- Pleim, J. E., Ran, L., Appel, W., Shephard, M. W., and Cady-Pereira, K.: New bidirectional ammonia flux model in an air quality model coupled with an agricultural model, *J. Adv. Model. Earth Sy.*, 11, 2934–2957, <https://doi.org/10.1029/2019MS001728>, 2019.
- Powers, J. G., Klemp, J. B., Skamarock, W. C., Davis, C. A., Dudhia, J., Gill, D. O., Coen, J. L., Gochis, D. J., Ahmadov, R., Peckham, S. E., Grell, G. A., Michalakes, J., Trahan, S., Benjamin, S. G., Alexander, C. R., Dimego, G. J., Wang, W., Schwartz, C. S., Romine, G. S., Liu, Z., Snyder, C., Chen, F., Barlarge, M., Yu, M., and Duda, M.: The weather research and forecasting model: Overview, system efforts, and future directions, *B. Am. Meteorol. Soc.*, 98, 1717–1737, <https://doi.org/10.1175/BAMS-D-15-00308.1>, 2017.
- Putman, W. M. and Lin, S.-J.: Finite-volume transport on various cubed-sphere grids, *J. Comput. Phys.*, 227, 55–78, <https://doi.org/10.1016/j.jcp.2007.07.022>, 2007.
- Pye, H. O. T., Pinder, R. W., Piletic, I., Xie, Y., Capps, S. L., Lin, Y.-H., Surratt, J. D., Zhang, Z., Gold, A., Luecken, D. J., Hutzell, W. T., Jaoui, M., Offenberg, J. H., Kleindienst, T. E., Lewandowski, M., and Edney, E. O.: Epoxide pathways improve model predictions of isoprene markers and reveal key role of acidity in aerosol formation, *Environ. Sci. Technol.*, 47, 11056–11064, <https://doi.org/10.1021/es402106h>, 2013.

- Pye, H. O. T., Murphy, B. N., Xu, L., Ng, N. L., Carlton, A. G., Guo, H., Weber, R., Vasilakos, P., Appel, K. W., Budisulistiorini, S. H., Surratt, J. D., Nenes, A., Hu, W., Jimenez, J. L., Isaacman-VanWertz, G., Misztal, P. K., and Goldstein, A. H.: On the implications of aerosol liquid water and phase separation for organic aerosol mass, *Atmos. Chem. Phys.*, 17, 343–369, <https://doi.org/10.5194/acp-17-343-2017>, 2017.
- Ran, L., Cooter, E., Benson, V., and He, Q.: Development of an agricultural fertilizer modeling system for bi-directional ammonia fluxes in the CMAQ model, edited by: Steyn, D. G. and Castelli, S. T., *Air Pollution Modeling and its Application XXI*, Chapter 36, Dordrecht, Springer, 213–219, [https://doi.org/10.1007/978-94-007-1359-8\\_36](https://doi.org/10.1007/978-94-007-1359-8_36), 2011.
- Ran, L., Pleim, J., Gilliam, R., Binkowski, F. S., Hogrefe, C., and Band, L.: Improved meteorology from an updated WRF/CMAQ modeling system with MODIS vegetation and albedo, *J. Geophys. Res.-Atmos.*, 121, 2393–2415, <https://doi.org/10.1002/2015JD024406>, 2016.
- Rogers, E., Black, T., Deaven, D., DiMego, G., Zhao, Q., Baldwin, M., Junker, N. W., and Lin, Y.: Changes to the operational “early” Eta Analysis/Forecast System at the National Centers for Environmental Prediction, *Weather Forecast.*, 11, 391–413, [https://doi.org/10.1175/1520-0434\(1996\)011<0391:CTTOEA>2.0.CO;2](https://doi.org/10.1175/1520-0434(1996)011<0391:CTTOEA>2.0.CO;2), 1996.
- Sarwar, G., Fahey, K., Napelenok, S., Roselle, S., and Mathur, R.: Examining the impact of CMAQ model updates on aerosol sulfate predictions, The 10th Annual CMAS Models-3 User’s Conference, 24–26 October 2011, Chapel Hill, NC, 2011.
- Sarwar, G., Gantt, B., Foley, K., Fahey, K., Spero, T. L., Kang, D., Mathur, R., Foroutan, H., Xing, J., Sherwen, T., and Saiz-Lopez, A.: Influence of bromine and iodine chemistry on annual, seasonal, diurnal, and background ozone: CMAQ simulations over the Northern Hemisphere, *Atmos. Environ.*, 213, 395–404, <https://doi.org/10.1016/j.atmosenv.2019.06.020>, 2019.
- Schwede, D., Pouliot, G. A., and Pierce, T.: Changes to the Biogenic Emissions Inventory System Version 3 (BEIS3), in: Proceedings of the 4th CMAS Models-3 Users’ Conference, 26–28 September 2005, Chapel Hill, NC, 2005.
- Sillman, S.: The use of NO<sub>y</sub>, H<sub>2</sub>O<sub>2</sub>, and HNO<sub>3</sub> as indicators for ozone-NO<sub>x</sub>-hydrocarbon sensitivity in urban locations, *J. Geophys. Res.-Atmos.*, 100, 14175–14188, <https://doi.org/10.1029/94JD02953>, 1995.
- Sillman, S.: The relation between ozone, NO<sub>x</sub> and hydrocarbons in urban and polluted rural environments, *Atmos. Environ.*, 33, 1821–1845, [https://doi.org/10.1016/S1352-2310\(98\)00345-8](https://doi.org/10.1016/S1352-2310(98)00345-8), 1999.
- Sillman, S., Logan, J. A., and Wofsy, S. C.: The sensitivity of ozone to nitrogen oxides and hydrocarbons in regional ozone episodes, *J. Geophys. Res.*, 95, 1837–1852, <https://doi.org/10.1029/JD095iD02p01837>, 1990.
- Skamarock, W. C. and Klemp, J. B.: A time-split nonhydrostatic atmospheric model for weather research and forecasting applications, *J. Computat. Phys.*, 227, 3465–3485, <https://doi.org/10.1016/j.jcp.2007.01.037>, 2008.
- Skamarock, W. C., Klemp, J. B., Dudhia, J., Gill, D. O., Liu, Z., Berner, J., and Huang, X.: A Description of the Advanced Research WRF Model Version 4 (No. NCAR/TN-556+STR), <https://doi.org/10.5065/1dfh-6p97>, 2019.
- Sofiev, M., Ermakova, T., and Vankevich, R.: Evaluation of the smoke-injection height from wild-land fires using remote-sensing data, *Atmos. Chem. Phys.*, 12, 1995–2006, <https://doi.org/10.5194/acp-12-1995-2012>, 2012.
- Stajner, I., Davidson, P., Byun, D., McQueen, J., Draxler, R., Dickerson, P., and Meagher, J.: US National Air Quality Forecast Capability: Expanding Coverage to Include Particulate Matter, Springer, Dordrecht, 379–384, [https://doi.org/10.1007/978-94-007-1359-8\\_64](https://doi.org/10.1007/978-94-007-1359-8_64), 2011.
- Sun, J., Fu, J. S., Huang, K., and Gao, Y.: Estimation of future PM<sub>2.5</sub>- and ozone-related mortality over the continental United States in a changing climate: An application of high-resolution dynamical downscaling technique, *J. Air Waste Manage.*, 65, 611–623, <https://doi.org/10.1080/10962247.2015.1033068>, 2015.
- Tang, Y., Lee, P., Tsidulko, M., Huang, H.-C., McQueen, J., DiMego, G. J., Emmons, L. K., Pierce, R. B., Thompson, A. M., Lin, H.-M., Kang, D., Tong, D., Yu, S., Mathur, R., Pleim, J. E., Otte, T. L., Pouliot, G., Young, J. O., Schere, K. L., Davidson, P. M., and Stajner, I.: The impact of chemical lateral boundary conditions on CMAQ predictions of tropospheric ozone over the continental United States, *Environ. Fluid Mech.*, 9, 43–58, <https://doi.org/10.1007/s10652-008-9092-5>, 2009.
- Tang, Y., Chai, T., Pan, L., Lee, P., Tong, D., Kim, H.-C., and Chen, W.: Using optimal interpolation to assimilate surface measurements and satellite AOD for ozone and PM<sub>2.5</sub>: A case study for July 2011, *J. Air Waste Manage.*, 65, 1206–1216, <https://doi.org/10.1080/10962247.2015.1062439>, 2015.
- Tang, Y., Bian, H., Tao, Z., Oman, L. D., Tong, D., Lee, P., Campbell, P. C., Baker, B., Lu, C.-H., Pan, L., Wang, J., McQueen, J., and Stajner, I.: Comparison of chemical lateral boundary conditions for air quality predictions over the contiguous United States during pollutant intrusion events, *Atmos. Chem. Phys.*, 21, 2527–2550, <https://doi.org/10.5194/acp-21-2527-2021>, 2021.
- Tewari, M., Chen, F., Wang, W., Dudhia, J., LeMone, M. A., Mitchell, K., Ek, M., Gayno, G., Wegiel, J., and Cuenca, R. H.: Implementation and verification of the unified NOAA land surface model in the WRF model, 20th Conference on Weather Analysis and Forecasting/16th Conference on Numerical Weather Prediction, Seattle, WA, 14 January 2004, [https://ams.confex.com/ams/84Annual/techprogram/paper\\_69061.htm](https://ams.confex.com/ams/84Annual/techprogram/paper_69061.htm) (last access: 6 April 2022) 2004.
- Tong, D. Q., Lee, P., and Saylor, R. D.: New Direction: The need to develop process-based emission forecasting models, *Atmos. Environ.*, 47, 560–561, <https://doi.org/10.1016/j.atmosenv.2011.10.070>, 2012.
- Tong, D. Q., Wang, J. X. L., Gill, T. E., Lei, H., and Wang, B.: Intensified dust storm activity and Valley fever infection in the southwestern United States, *Geophys. Res. Lett.*, 44, 4304–4312, <https://doi.org/10.1002/2017GL073524>, 2017.
- Troen, I. and Mahrt, L.: A simple model of the atmospheric boundary layer: Sensitivity to surface evaporation, *Bound.-Lay. Meteorol.*, 37, 129–148, <https://doi.org/10.1007/BF00122760>, 1986.
- US EPA Office of Research and Development: CMAQv5.0.2 (Version 5.0.2), Zenodo [data set], <https://doi.org/10.5281/zenodo.1079898>, 2014.
- US EPA Office of Research and Development: CMAQ (Version 5.3.1), Zenodo [data set], <https://doi.org/10.5281/zenodo.3585898>, 2019.



- Vukovich, J. M. and Pierce, T.: The Implementation of BEIS3 within the SMOKE modeling framework, *Environ. Sci.*, 2002.
- Weiss, A. and Norman, J.: Partitioning solar radiation into direct and diffuse, visible and nearinfrared components, *Agr. Forest Meteorol.*, 34, 205–213, [https://doi.org/10.1016/0168-1923\(85\)90020-6](https://doi.org/10.1016/0168-1923(85)90020-6), 1985.
- Westerling A. L., Hidalgo, H. G., Cayan, D. R., and Swetnam, T. W.: Warming and earlier spring increase western US forest wildfire activity, *Science*, 313, 940–943, <https://doi.org/10.1126/science.1128834>, 2006.
- Wilkins, J., Pouliot, G., Pierce, T., and Beidler, J.: Exploring the Vertical Distribution of Wildland Fire Smoke in CMAQ, 2019 International Emissions Inventory Conference, 28 July–2 August 2019, Dallas, Texas, [https://cfpub.epa.gov/si/si\\_public\\_record\\_report.cfm?Lab=NERL&dirEntryId=346294](https://cfpub.epa.gov/si/si_public_record_report.cfm?Lab=NERL&dirEntryId=346294) (last access: 6 April 2022), 2019.
- Williams, A. P., Cook, E. R., Smerdon, J. E., Cook, B. I., Abatzoglou, J. T., Bolles, K., Baek, S. H., Badger, A. M., and Livneh, B.: Large contribution from anthropogenic warming to an emerging North American megadrought, *Science*, 368, 314–318, <https://doi.org/10.1126/science.aaz9600>, 2020.
- Williams, J. R.: The EPIC model, in: Computer models in watershed hydrology, edited by: Singh, V. P., Chapter 25, 909–1000, Littleton, CO, Water Resources Publications, ISBN-13 978-0-918334-91-6, 1995.
- World Health Organization (WHO): Air Quality Guidelines, Global update 2005, Particulate matter, ozone, nitrogen dioxide and sulfur dioxide, ISBN 92-890-2192-6, 2006.
- World Health Organization (WHO): WHO Guidelines for Indoor Air Quality: Selected Pollutants, World Health Organization, Regional Office for Europe Scherfigsvej 8, 2100 Copenhagen, Denmark, ISBN 9789289002134, 2010.
- Yang, F., Tallapragada, V., Kain, J. S., Wei, H., Yang, R., Yudin, V. A., Moorthi, S., Han, J., Hou, Y. T., Wang, J., Treadon, R., and Kleist, D. T.: Model Upgrade Plan and Initial Results from a Prototype NCEP Global Forecast System Version 16, 2020 AMS Conference, Boston, MA, 15 January 2020, <https://ams.confex.com/ams/2020Annual/webprogram/Paper362797.html> (last access: 6 April 2022), 2020.
- Yarwood, G., Whitten, G. Z., and Jung, J.: Final Report. Development, Evaluation and Testing of Version 6 of the Carbon Bond Chemical Mechanism (CB6), 22 September 2010, ENVIRON International Corporation, 06-17477Y, <https://www.tceq.texas.gov/assets/public/implementation/air/am/contracts/reports/pm/5820784005FY1026-20100922-environ-cb6.pdf> (last access: 6 April 2022), 2010.
- Zeka A., Zanobetti, A., and Schwartz, J.: Short term effects of particulate matter on cause specific mortality: effects of lags and modification by city characteristics, *Occup. Environ. Med.*, 62, 718–725, <https://doi.org/10.1136/oem.2004.017012>, 2006.
- Zhang, X., Kondragunta, S., Ram, J., Schmidt, C., and Huang, H.-C.: Near-real-time global biomass burning emissions product from geostationary satellite constellation, *J. Geophys. Res.-Atmos.*, 117, D14201, <https://doi.org/10.1029/2012JD017459>, 2012.
- Zhang, X., Kondragunta, S., and Roy, D. P.: Interannual variation in biomass burning and fire seasonality derived from geostationary satellite data across the contiguous United States from 1995 to 2011, *J. Geophys. Res.-Biogeo.*, 119, 1147–1162, <https://doi.org/10.1002/2013JG002518>, 2014.
- Zhang, Y., Vijayaraghavan, K., Wen, X.-Y., Snell, H. E., and Jacobson, M. Z.: Probing into regional ozone and particulate matter pollution in the United States: 1. A 1 year CMAQ simulation and evaluation using surface and satellite data, *J. Geophys. Res.*, 114, D22304, <https://doi.org/10.1029/2009JD011898>, 2009a.
- Zhang, Y., Wen, X.-Y., Wang, K., Vijayaraghavan, K., and Jacobson, M. Z.: Probing into regional ozone and particulate matter pollution in the United States: 2. An examination of formation mechanisms through a process analysis technique and sensitivity study, *J. Geophys. Res.*, 114, D22304, <https://doi.org/10.1029/2009JD011898>, 2009b.
- Zhang, Y., Bocquet, M., Mallet, V., Seigneur, C., and Baklanov, A.: Real-time air quality forecasting, part I: History, techniques, and current status, *Atmos. Environ.*, 60, 632–655, <https://doi.org/10.1016/j.atmosenv.2012.06.031>, 2012a.
- Zhang, Y., Bocquet, M., Mallet, V., Seigneur, C., and Baklanov, A.: Real-time air quality forecasting, part II: State of the science, current research needs, and future prospects, *Atmos. Environ.*, 60, 656–676, <https://doi.org/10.1016/j.atmosenv.2012.02.041>, 2012b.
- Zhang, Y., West, J. J., Mathur, R., Xing, J., Hogrefe, C., Roselle, S. J., Bash, J. O., Pleim, J. E., Gan, C.-M., and Wong, D. C.: Long-term trends in the ambient PM<sub>2.5</sub>- and O<sub>3</sub>-related mortality burdens in the United States under emission reductions from 1990 to 2010, *Atmos. Chem. Phys.*, 18, 15003–15016, <https://doi.org/10.5194/acp-18-15003-2018>, 2018.
- Zhao, H., Zheng, Y., and Li, T.: Air Quality and Control Measures Evaluation during the 2014 Youth Olympic Games in Nanjing and its Surrounding Cities, *Atmosphere*, 8, 8060100, <https://doi.org/10.3390/atmos8060100>, 2017.
- Zhou, L., Lin, S., Chen, J., Harris, L. M., Chen, X., and Rees, S. L.: Toward Convective-Scale Prediction within the Next Generation Global Prediction System, *B. Am. Meteorol. Soc.*, 100, 1225–1243, <https://doi.org/10.1175/BAMS-D-17-0246.1>, 2019.
- Zhou, T., Sun, J., and Yu, H.: Temporal and Spatial Patterns of China's Main Air Pollutants: Years 2014 and 2015, *Atmosphere*, 8, 8080137, <https://doi.org/10.3390/atmos8080137>, 2017.